Ultra Hard Mount Active Vibration Control

Improving the performance of ultra hard mount systems using active vibration control strategies

M.J. Neele

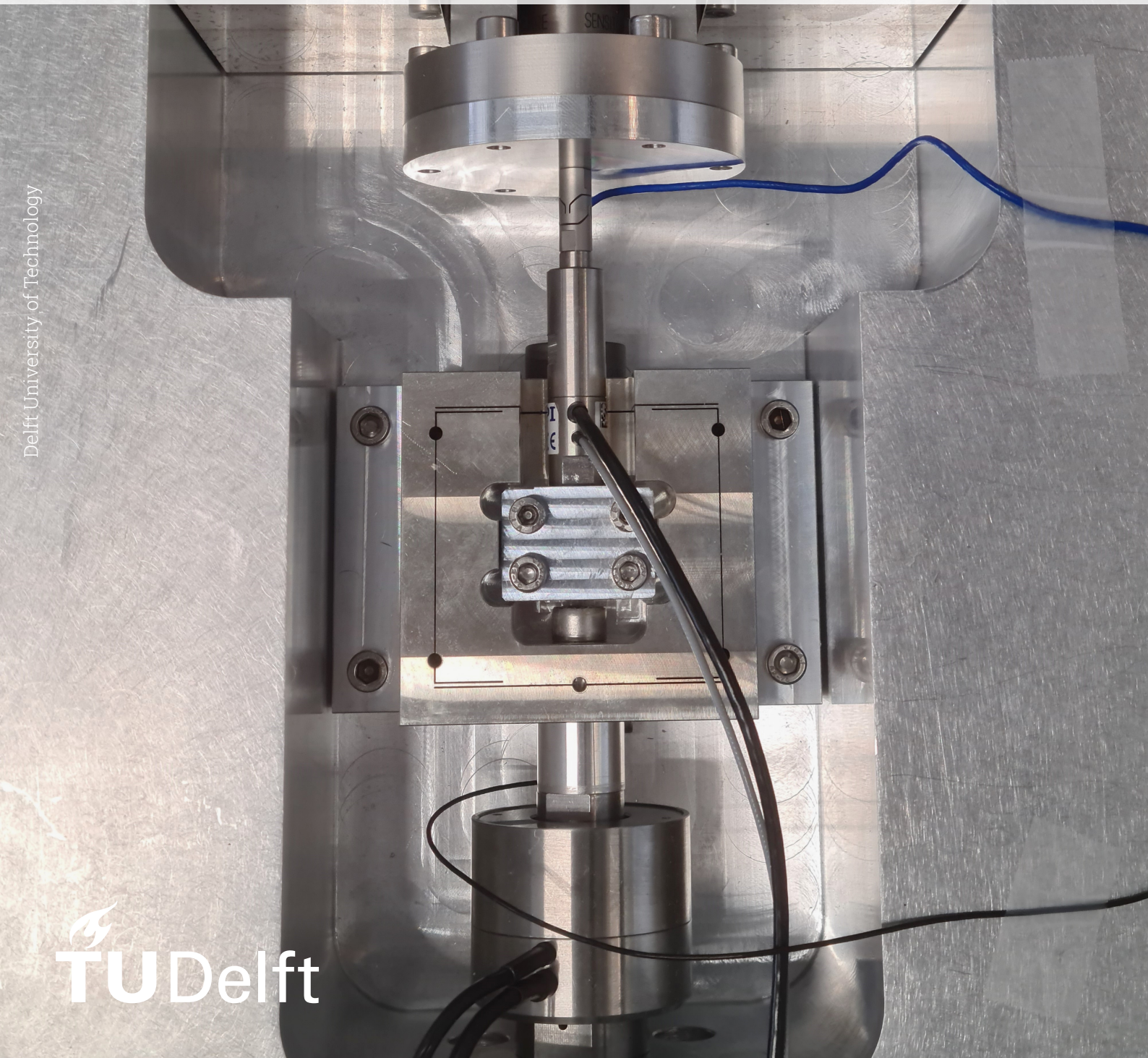

Delft University of Technology

TU Delft

Ultra Hard Mount Active Vibration Control

Improving the performance of ultra hard mount systems using active vibration control strategies

by

M.J. Neele

Senior Supervisor:	Hassan Hossein Nia Kani
Daily Supervisor:	Marcin Kaczmarek
Company Supervisor	Jonas Reiser
Faculty:	Faculty of Mechanical Engineering, Delft

Cover: Close-up of the piezo-stack actuators inside the experimental setup, used for active vibration control.

TU Delft

Summary

High-precision mechatronic equipment often benefits from or even needs vibration isolation to function within specification. Examples of such equipment include metrology devices, space instrumentation and lithography assemblies. Vibration isolation is often the function of the mounting between the equipment and the floor or rest of the machine. An important factor for vibration isolation is the stiffness of this mount. High stiffness mounts result in high force disturbance rejection, at the cost of sensitivity to indirect disturbances. So-called ultra hard mount systems take advantage of ultra high stiffness to offer superior position stability in the presence of force disturbances. However, this also leads to an emphasized sensitivity to indirect disturbances. Active vibration control can be used to overcome this. Feedback is used to dampen the resonance mode of the mounting system. Feedforward is used to lower the transmissibility, resulting in reduced sensitivity to indirect disturbances. This has been successfully implemented on less stiff hard mount systems in the past, but the techniques remained unexplored on ultra hard mount systems. This research focusses on the experimental implementation of existing active vibration control techniques on an ultra hard mount system. It was found that the closed loop behaviour of piezo-based ultra hard mount systems are well predictable. Furthermore, it was found that good damping performance can be achieved by various methods, reducing the output vibrations up to 60%. Using straightforward stiffness compensation feedforward, the influence of indirect disturbances was shown to be reduced significantly. A reduction of 94% in the effect of indirect disturbances was realized using disturbance feedforward when compared to the uncontrolled case. This work shows that ultra hard mounts can be used in applications where strong direct disturbance rejection is required, even in the presence of indirect disturbances using a combined feedback and feedforward approach.

Contents

1 Introduction

Almost everybody in the world owns multiple devices containing numerous tiny chips and sensors. To increase the capabilities of these devices while still keeping them small, lightweight, and energy efficient, the components are becoming smaller. This increases the precision demands of the machines fabricating these chips, sensors, and other components. However, at the same time it is important to keep the costs of parts low. Low parts cost means affordable, and thus accessible, electronics. To keep the costs of parts down, throughput has to be high. High throughput means an increase in operating speeds and thus higher accelerations of moving parts. Consequently, while the error margin decreases due to demands on precision, there is an increase in the vibrations from machine operation limiting precision [1]. This conflict between speed and precision does not only occur in the semiconductor industry, similar increasing demands can be found in the medical sector and the space industry.

In order to meet such precision or throughput targets, there is a need to reduce the effect of vibrations. Disturbances can be classified into two distinct categories based on how they enter a system: direct disturbances, mentioned above which act directly on the equipment as a force, and indirect disturbances, which enter the equipment through the mountings as a displacement [7]. Sources of disturbances are highly application specific. Sources of direct disturbances include accelerating stages, forces transmitted through cables, acoustic excitation and electronic noise resulting in actuator movement. Direct disturbances are also commonly called force disturbances. Although the dynamics are similarly application specific, a typical profile is shown in figure 1.1a. Indirect disturbances are commonly caused by floor vibrations and are thus often referred to as such. Work has been done to categorize floor vibrations into so-called 'Vibration-Criteria' curves based on the magnitude of the vibrations [6]. Each curve corresponds to levels of floor vibration acceptable for different applications, ranging from a VC-A curve for optical telescopy up to 400X to VC-G for extremely quiet research spaces [8]. In this work the VC-C curve is used, shown in figure 1.1a, described as a good standard for lithography and inspection equipment to 1 micrometer detail size.

Vibration isolation is generally the role of the mount between equipment and machine frame or floor. A model of such a mounting system can be found in figure 1.1b. Here the equipment that is to be isolated is shown as a mass m. The mounting is abstracted as a spring and damper with stiffness k and damping coefficient c. If such a system is designed specifically with disturbance rejection in mind it is often called a vibration isolation system. Direct disturbances are denoted by a force F_d and indirect disturbances by displacement x_1 and acceleration $\ddot{x}_1$. The motion of the isolated equipment, x_2 and $\ddot{x}_2$ in figure 1.1b, will be referred to as the output of the vibration isolation system. Vibration isolation systems are used in a variety of applications. Metrology equipment like atomic force microscopes [2], space instrumentation like telescopes or other optical instruments in orbit [3, 4], and lithography assemblies such as the exposure system [5] all benefit from, or even need vibration isolation systems to operate within specification.

For vibration control, the transfer functions from direct and indirect disturbances to the motion of isolated equipment are especially important. These transfer functions are called the *compliance*, from

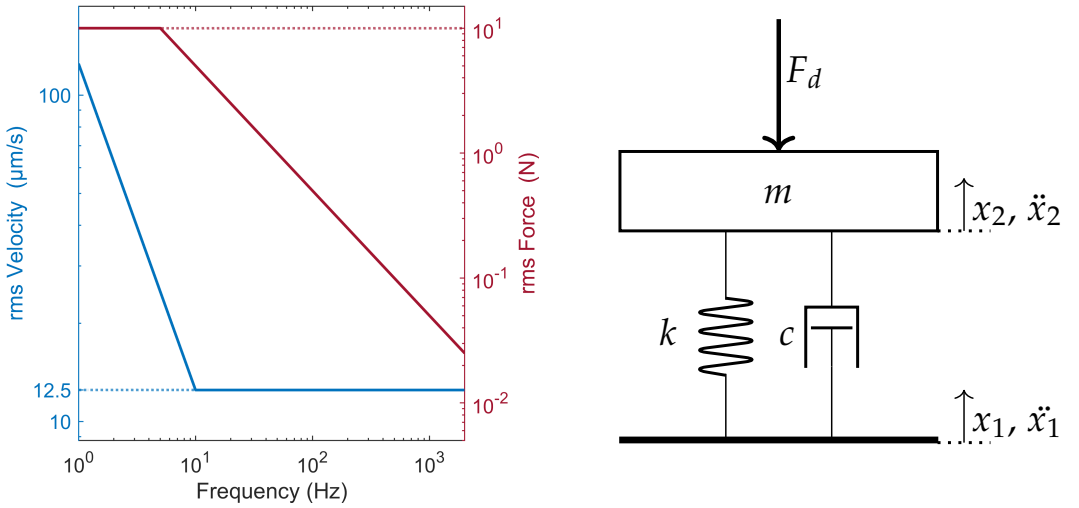

(a) Typical dynamics of disturbances acting on a system. The left axis shows an indirect disturbance profile (VC-C curve from [6]) in terms of rms velocity, the right axis shows a direct disturbance profile.

(b) A simplified, single degree of freedom abstraction of the mounting system. The isolated system with mass m, is subjected to direct disturbance F_d. The isolation system has a stiffness k and damping c. An indirect disturbance $x_1, \ddot{x}_1$ acts on the system.

Figure 1.1: A simplified model of a (passive) vibration isolation system and the disturbances that may act on such a system.

direct disturbance to output, and the *transmissibility*, from indirect disturbance to output [9]. It is desired that the response of these two is as low as possible, as this means that the disturbances have little influence on the output.

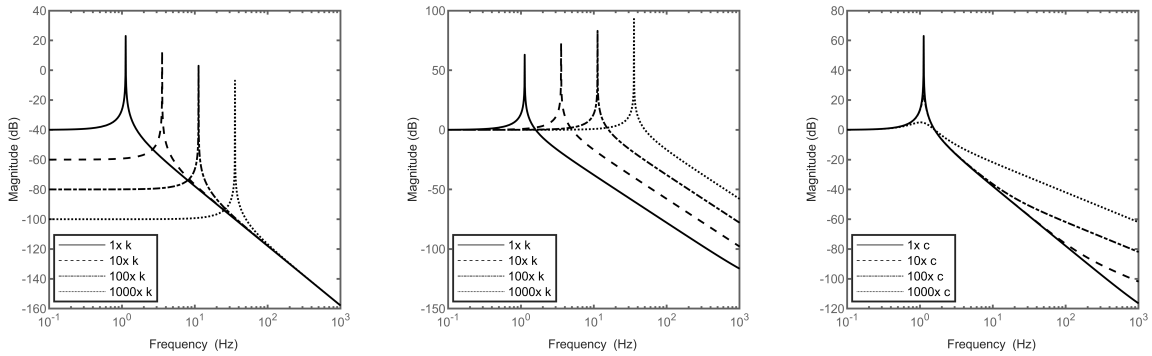

(a) Influence of stiffness on the compliance

(b) Influence of stiffness on the transmissibility

(c) Influence of damping on the transmissibility

Figure 1.2: The influence of system mount design choices, stiffness k and damping c, on the transmissibility and compliance of the mounting system. A higher stiffness results in low compliance, meaning good direct disturbance rejection, but a high resonance frequency, resulting in worsened indirect disturbance attenuation. An increase in damping leads to a lower resonance peak, at the cost of decreased high frequency disturbance rejection.

When designing a mount for vibration control the design choices of stiffness and compliance are important. These influence the dynamic behaviour of the mount and thus its compliance and transmissibility. The effect of stiffness on the compliance is plotted in figure 1.2a. It can be seen an increase in stiffness leads to a lower the compliance. A low compliance response means that the system is much less affected by direct disturbances. In figure 1.2b the influence on the transmissibility of increased stiffness is shown. It can be seen that an increase in stiffness results in a higher resonance frequency. A distinction between low stiffness 'soft' systems and higher stiffness 'hard' systems can be made based on the resonance frequency, or 'suspension frequency', of the mounting system. Soft mount systems have a suspension frequency below 5 Hz and hard mounts above 5 Hz [7].

Soft mount systems perform well in reducing the effect of indirect disturbances, as the desired attenuation by the low-pass behaviour of the structure starts at a low frequency. This results in broad-band isolation. However, the high compliance leads to poor direct disturbances rejection. Furthermore, sagging and misalignment issues caused by the low stiffness, impose the need for additional leveling systems. This increases complexity and leads to slow settling times as these levelling systems have low control bandwidth [10].

Hard mounts have been proposed to solve the issues of soft mount systems [11]. Use of higher stiffness reduces the sensitivity to force disturbances, increase position stability, and absolve the need for complex and slow levelling systems. These advantages come at the cost of worsened indirect disturbance rejection due to the higher resonance frequency. The high resonance frequency means that there is a wider frequency band of indirect disturbances that enter the system unattenuated by the structure.

Another important property of the mounting system is the damping. The influence of increased damping on the transmissibility is shown in figure 1.2c. It can be seen that an increase in damping leads to a decrease in the magnitude of the resonance peak. However, it also leads to a significant decrease in high frequency attenuation. Therefore, it is preferred to have low passive damping and add damping artificially with use of Active Vibration Control (AVC) [12, 13].

Active vibration control makes use of active components such as sensors and actuators to improve the mounting dynamics. The most common method is 'sky-hook' damping, utilizing velocity feedback to dampen resonance modes [14]. This technique can also be applied with different sensor types like accelerometers or force sensors [15, 16, 17]. When position-related measurements are available, Positive Position Feedback [18] can be used. Furthermore, disturbance feedforward techniques can be employed to effectively lower the transmissibility [10, 19]. Instead of measuring the motion of the isolated equipment as is done with feedback, disturbance feedforward directly measures the incoming floor vibrations. By calculating an opposing force the floor vibrations can be largely cancelled, resulting in a lowered transmissibility.

In applications where direct disturbances are large and position stability is especially important it may be beneficial to have even stiffer supports than the aforementioned hard mounts. Such ultra hard mount systems offer superior force disturbance rejection. These mounts can be made from piezoelectric stack actuators [21]. Added benefits of using piezo-based actuators, as opposed to Lorentz based solutions, are low energy consumption in static operation, high possible actuation forces and accelerations, and no magnetic fields that can interfere with sensitive equipment [22]. Although the direct disturbance rejection advantages of high stiffness are emphasized, so is the sensitivity to floor vibrations.

A preliminary study was conducted by the Piezo Drives & Systems Technology group of Physik Instrumente (PI) to investigate the viability of using piezo-based active damping on a larger hexapod structure. It was found that good damping of the first four modes of the system was possible using velocity control in an experimental setup. This preliminary study showed that a piezo-based ultra stiff active mounting system could be a feasible solution for applications demanding strong direct disturbance rejection.

1.1. Problem Statement and Research Objectives

Ultra hard mount systems promise excellent direct disturbance rejection performance but remain mostly unexplored. Many different active vibration control feedback techniques have been proposed in the past but are mostly implemented on softer systems. Most feedback methods remain unexplored on ultra hard mount systems. Additionally, techniques are often introduced compared to open loop wile an extensive comparison between different methods is lacking. The main downside of high stiffness systems is their susceptibility to indirect disturbances. Disturbance feedforward techniques have been developed on hard mount systems to address this issue, but the feasibility on piezo based ultra hard mounts remains unexplored. Overall, the performance of ultra hard mount systems for vibration control remains largely uninvestigated.

This thesis explores the performance of active vibration control on ultra-hard mount systems by investigating the following research objectives:

- *Experimentally analyse and compare the influence of different active vibration control techniques on the performance of an ultra hard mount system.*
- *Investigate the feasibility of disturbance feedforward on an ultra hard mount system as a way to lower its sensitivity to indirect disturbances.*

The first objective will show if existing active vibration control methods may be effectively adapted to ultra stiff systems, what factors influence the real world performance of ultra high stiffness systems, and how much performance may be gained by using different feedback strategies. The second objective will show if disturbance feedforward can reduce the influence of indirect disturbances, thereby enabling the use of ultra hard mounts in applications with indirect disturbances present.

In this introductory chapter background information on mounting design and vibration isolation is provided and the investigation into ultra hard mount systems is motivated. The following chapter presents the paper resulting from this work, which has been submitted to the IEEE/ASME MESA 2024 conference. In chapter 3, more details not included in the paper regarding the experimental results are given. Simulation results are discussed, the influence of controller gain is analysed, the experimental damping results are given and finally disturbance feedforward is elaborated upon. In chapter 4, the work is summarized and conclusions are provided and recommendations regarding future work building on this research are given.

Additionally, in Appendix A detailed information regarding the experimental setup and LabView is given. Some additional results and the performance with a slightly different disturbance case may be found in Appendices B and C. Finally, more in-depth explanations of Dynamic Error Budgeting and using the DEB method for optimization can be found in Appendix D.

Experimental Evaluation of Ultra Hard Mount Vibration Control Systems

Maurits Neele
Precision and Microsystems Engineering
Delft University of Technology
Delft, the Netherlands

Marcin B. Kaczmarek
Precision and Microsystems Engineering
Delft University of Technology
Delft, the Netherlands

Jonas Reiser
Piezo Drives & Systems Technology
Physik Instrumente (PI) GmbH & Co.KG
Karlsruhe, Germany

Mathias Winter
Piezo Drives & Systems Technology
Physik Instrumente (PI) GmbH & Co.KG
Karlsruhe, Germany

S. Hassan HosseinNia
Precision and Microsystems Engineering
Delft University of Technology
Delft, the Netherlands

***Abstract*—In this paper the performance of an ultra hard mount active vibration control system is evaluated. High stiffness mounts offer position stability and high force disturbance rejection, at the cost of sensitivity to indirect disturbances. Active vibration control can be used to overcome this, using feedback to dampen the resonance and feedforward for lowered transmissibility. This paper evaluates different feedback strategies and compares experimentally on a single-axis piezo-based ultra hard mount system. It was found that good damping performance can be achieved, reducing the output vibrations by almost 60% with various feedback methods. Furthermore, using straightforward stiffness compensation feedforward, the influence of indirect disturbances was shown to be reduced significantly. The influence of indirect disturbances was reduced by 94% with feedforward when compared to the uncontrolled case.**

***Index Terms*—Active vibration control, Vibration isolation, Disturbance feedforward control, Disturbance rejection, Hard mount, Piezoelectric stack,**

I. Introduction

The performance of high-precision machines and scientific instruments depends on the disturbances acting on them. While the nature and dynamics of such disturbances are highly case-specific, they can be divided into two classes. Indirect disturbances are commonly floor vibrations and are thus often referred to as such. Direct disturbances may be caused by the forces acting directly on a system, forces transmitted through cables, and motion of systems components [1].

Coping with the disturbances is often the role of the mount between the device and the machine's frame or the floor. When the floor vibrations are the primary concern, the mount can be designed as a soft vibration isolation system [2]. The low stiffness and the corresponding low resonance frequency of the system (typically below 5Hz) are advantageous in this context, as above the resonance, the transmissibility of vibration is attenuated. This, however, comes at the cost of problems with levelling, sagging and increased force disturbance sensitivity [3]. Hard mounts have been proposed to address these issues [1]. Using a higher stiffness mount leads to much-decreased sensitivity to direct disturbances [4] and a higher resonance frequency of the system, reaching 35 Hz [3]. In consequence, the system is more susceptible to indirect vibrations.

In this paper, we focus on applications where the direct disturbances acting on the system are large and position stability is especially important. To assure it, an *ultra hard* mount based on piezoelectric stack actuators is proposed. Thanks to their capability of exerting high forces, an active solution can be created to deal with both direct and indirect disturbances effectively. Additionally, piezoelectric stacks are proven technology in the high-tech industry, have low energy consumption in static operation, and produce no magnetic fields that can interfere with sensitive equipment [5].

The high stiffness of the piezoelectric stack prevents the excitation of the structure by direct disturbances. The performance is further improved by active damping of the resonance peak. The most common method is 'sky-hook' damping, utilizing velocity feedback to dampen resonance modes [6]. This technique can also be applied with different sensor types like accelerometers or force sensors [1, 7]. When position-related measurements are available, Positive Position Feedback [8] can be used to avoid differentiation and noise amplification. While the active damping methods are well-developed and commonly used, extensive studies comparing them to each other are missing.

Because of the high resonance frequency, the system's passive structure is ineffective in isolating the floor vibrations. However, the influence of indirect vibrations can be cancelled actively using feedforward techniques based on the measurement of the incoming floor vibrations [9]. Feedforward requires an accurate dynamic model of the system which can be difficult to acquire in practice [10], as such work has focused on adaptive feedforward techniques [3, 11]. So far

This work was supported by the NWO HTSM Applied and Technical Science Program under project MetaMech with number 17976.

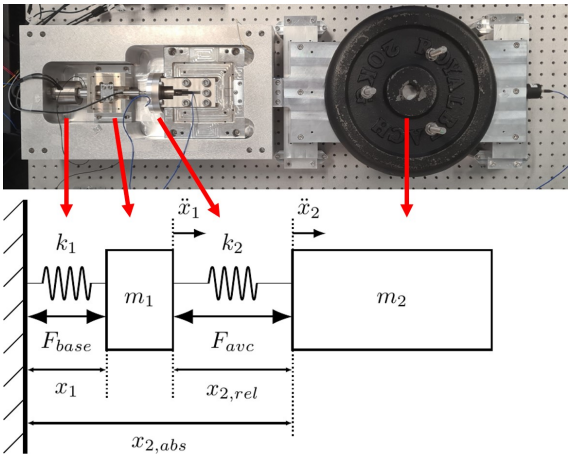

(a) Top-down overview of the experimental setup, with corresponding mass-spring damper model.

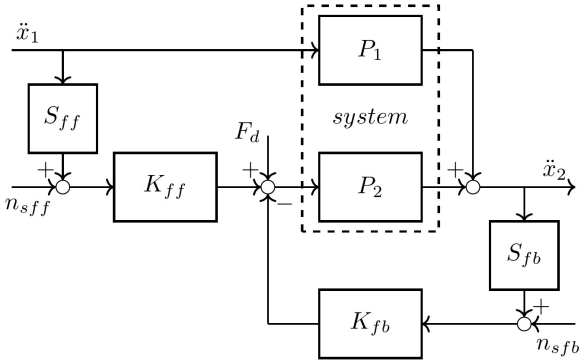

(b) Block-diagram representation of an active vibration control system, showing both feedback and feedforward controllers.

Fig. 1: The piezo-based experimental set-up used for evaluation of different active vibration control methods.

the feedforward techniques have been applied in hard mounts, but their effectiveness in high-stiffness piezoelectric systems has not been investigated.

The objective of this work is to experimentally evaluate the performance of ultra hard mounts in the vibration control context. The problem under study is formally presented in Section 2, together with preliminary information. Section 3 presents the results obtained from the experiments. The paper is concluded in Section 4.

II. System description

A single-axis experimental setup, presented in Fig.1a, is used to represent the ultra hard mount system. A platform with adjustable mass represents the payload to be supported. The main stack actuator (model *P-843.20*) has a stiffness of 27×10^6 N/m, and constitutes the ultra hard mount and connects the payload to the shaking base. This shaking base is actuated by another stack actuator (model *P-235.1S*), with a higher stiffness of 860×10^6 N/m. Motion of all elements of the setup is constrained to a single degree of freedom using flexures. The abstraction of the setup is also presented in Fig. 1a. Accelerations $\ddot{x}_1, \ddot{x}_2$ are measured using *PCB Synotech 393B05* accelerometers. Absolute displacement of m_1 is measured with a *PIseca D-510.021* and the the absolute displacement of m_2 with a *D-050* capacitive sensor. Finally, relative measurements are taken with the integrated strain gauge sensors of the stack actuators. In the configuration used in this paper, the resonance frequency of the system is 103 Hz. This can be adjusted to a higher or lower frequency by adjusting the mass m_2.

To study the response of a system to floor vibrations, a vibration profile based on the VC-C curve from [12] is applied to the shaking base. Direct disturbances are applied to the main stack actuator, also used for active vibration control, with the force profile starting at 10 N at low frequencies and descending with -1 slope from 5 Hz onwards.

Figure 1b shows the block diagram of the implemented control system with acceleration measurements. When absolute and relative positions are measured, similar structures are used. Transfer functions P_1 and P_2 represent the transmissibility and compliance of the passive structure, respectively. Transfer function K_{fb} represents the feedback controllers for active damping and K_{ff} corresponds to the feedforward controller's dynamics.

The goal of vibration control is to minimize the motion of the mass $\ddot{x}_2$. To calculate the total error, the Power Spectrum Density (PSD) of the signal is integrated to obtain the Cumulative Power Spectrum (CPS):

$$\mathrm{CPS}(f) = \int_0^f \mathrm{PSD}(v)\ \mathrm{d}v \tag{1}$$

The CPS visualizes the contribution to the total error at each frequency. The final value of the CPS is equal to the square of the root-mean-square (RMS) of the signal [13].

The reduction of the resonance peak by active damping is represented by the sensitivity function [14]

$$S = \frac{1}{1 + K_{fb}P_2}. \tag{2}$$

To prevent noise amplification and changing the dynamics of the system at other frequency regions, it should have a notch filter characteristics. Such characteristics are achieved with the triangular open-loop gain $K_{fb}P_2$ [15]. The differences between the different controllers implemented are shown in Fig. 2a. In the most common approach, velocity feedback (VFB) is used [6]. When accelerometers are used as sensors, the controller takes form of a low-pass filter

$$K_{vfb} = \frac{g}{s + \omega_v} \tag{3}$$

to avoid the drawbacks of using pure integrators. To decrease the influence of noise and excitation of high-frequency dynamics in the system a bandpass filter is added close to the

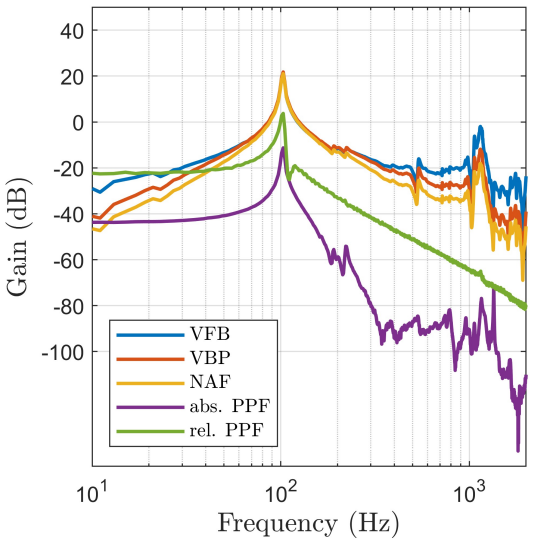

(a) Open-loop gain of the different AVC strategies. An optimal shape is a triangular shape centered on the resonance frequency.

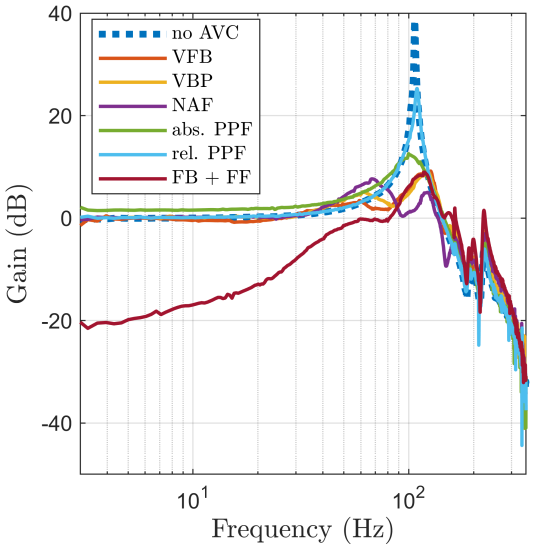

(b) Transmissibility from x_1 to x_2 of the system with no AVC and with different strategies implemented, showing the damping performance of the different methods.

Fig. 2: The open-loop gain and transmissibility plots of the different implemented strategies.

target frequency to be damped, forming Velocity Band-Pass feedback (VBP) controller

$$K_{vbp} = \frac{g\ \omega_{c1}\ \omega_{c2}}{(s+\omega_{c1})\ (s+\omega_{c2})}. \tag{4}$$

To achieve a stronger effect, a controller with a resonance peak

$$K_{naf} = \frac{g\ m\ \omega_f^2}{s^2+\zeta\ \omega_f\ s+\omega_f^2} \tag{5}$$

is used to increase the gain in the vicinity of the resonance to be damped in the Negative Acceleration Feedback (NAF) strategy [16, 17].

When position-related measurements are available, Positive Position Feedback (PPF) controllers with dynamics

$$K_{ppf} = \frac{g\ k\ \omega_f^2}{s^2+\zeta\ \omega_f\ s+\omega_f^2} \tag{6}$$

can be used to avoid differentiation of signals and noise amplification. This strategy can be used with both relative position between the isolated equipment and its mounts and absolute position, although the latter is much harder to measure in practice, requiring complicated separate measurement frames. The dynamics of the controller are the same for both relative and absolute PPF.

The feedforward controller is used to decrease the transmissibility of vibrations from the base of the mount. By calculating the system's reaction to the measured indirect disturbance, their effect can be diminished with an opposing control force. The most basic approach is stiffness compensation feedforward. With this method only the stiffness is accounted for and combined with a low-pass filter to avoid feeding noise into the system:

$$K_{ff} = -k\frac{\omega_{lp}}{s+\omega_{lp}}. \tag{7}$$

Note that the position of the base (x_1) is used for feedforward signal generation. For best results, feedback for active damping and feedforward are used simultaneously.

III. Experimental Evaluation Results

In this section, we discuss the performance of the considered AVC strategies tested on the hard mount system. The controllers were tuned based on rules from literature and experimental observations. The corner frequency of velocity feedback ω_v was set at 10 rad/s. The corner frequencies of the velocity band-pass controller ω_{c1}, ω_{c2} were set at half the resonance frequency and three times the resonance frequency as it was found this gave a good trade-off between damping and low noise amplification. The tuning of the negative acceleration controller was based on positive position feedback tuning from [18]. Tuning of both positive position feedback controllers was based on the tuning by [19]. The damping coefficient for relative position feedback was halved as experiments showed this improved performance. For each controller, the optimum gain was found by performing a gain sweep on the experimental setup.

The transmissibility with each strategy was measured by exciting the system and measuring the response from x_1 to x_2, with results plotted in Fig. 2b. The response in the absence of control is characterized by a sharp resonance peak at 103 Hz. All the tested strategies achieve a significant reduction

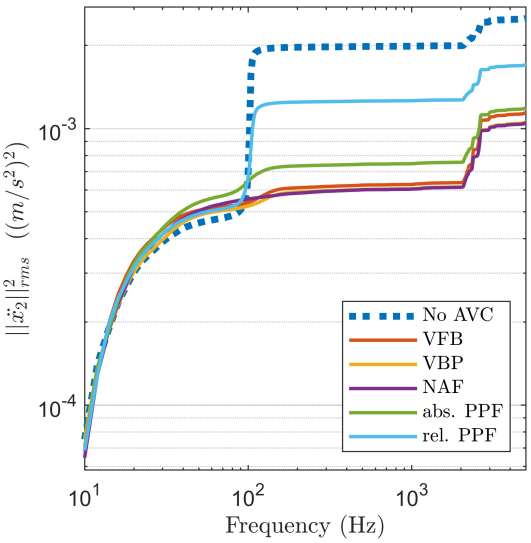

(a) CPS of $\ddot{x}_2$ showing the system response to direct and indirect disturbance excitation without AVC and with different feedback strategies implemented.

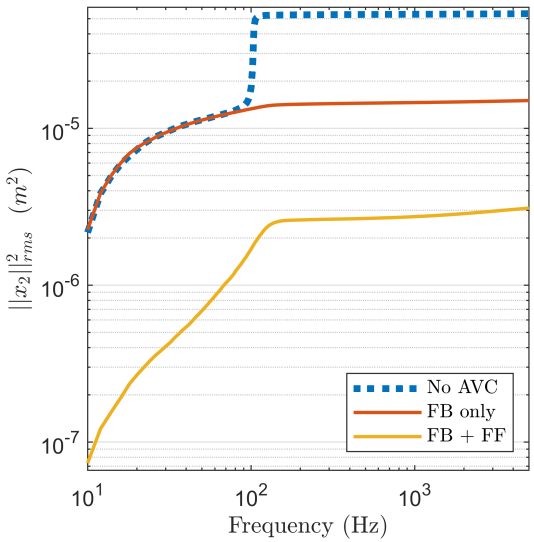

(b) CPS of x_2 showing the system response to indirect disturbance excitation without AVC, with only feedback, and feedback combined with stiffness compensation feedforward

Fig. 3: Cumulative Power Spectra obtained from the experimental results.

of the resonance peak, with the best results achieved using the acceleration-based methods (VFB, VBF, NAF). When PPF with absolute position measurement is used, base vibration transmission at low frequencies is amplified. A significant transmissibility reduction is obtained with the feedforward strategy. Due to the simplistic nature of the method used, it is mainly effective in a narrow range of frequencies. This, however, is sufficient to improve the performance of the system significantly, as will be demonstrated.

Fig. 3a shows the CPS of the response of the system to combined direct and indirect disturbances. Without control, large contributions are caused by the resonance peak at 103 Hz and high-frequency modes of the system around 1100 Hz. With active damping, the contribution of the resonance is significantly decreased. However, visible from the increase before the resonance frequency compared to the open-loop, the influence of the noise on the system is amplified. Furthermore, the high-frequency parasitic modes at around 1100 Hz are excited by the controllers, leading to a slight increase in vibrations. This shows the trade-off existing with these controllers: an increase in gain leads to both increased damping, amplified influence of noise and excitation of high-frequency modes. This behaviour limits the achievable reduction of vibrations.

The performance of the PPF using absolute position measurements approaches the performance of velocity feedback. This is achieved despite the amplification of the base-vibration transmissibility and smaller resonance peak reduction, thanks to smaller excitation of the high-frequency dynamics. Due the shape of the open-loop gain, visible in Fig. 2a, relative PPF is not able to achieve similar performance. It can be seen that relative PPF has high open-loop gain at low frequencies

TABLE I: Numerical results of experimental evaluation of different AVC feedback strategies showing the RMS of the acceleration of the isolated mass $\ddot{x}_2$ of each strategy and the percentage with respect to no AVC.

Method	RMS of $\ddot{x}_2$ (m/s^2)	% of No AVC
No AVC	2.5007e-03	100%
VFB	1.1426e-03	45.69%
VBP	1.0572e-03	42.27%
NAF	1.0489e-03	41.94%
abs. PPF	1.1877e-03	47.49%
rel. PPF	1.7018e-03	68.05%

TABLE II: Numerical results of experimental evaluation of indirect disturbance rejection with feedback and feedforward showing the RMS of the position of the isolated mass x_2 and the percentage with respect to no AVC.

Method	RMS of x_2 (m)	% of No AVC
No AVC	5.3778e-05	100%
FB only	1.5021e-05	27.93%
FB + FF	3.0984e-06	5.76%

without a significant peak at the resonance frequency. As a result, it is not possible to dampen the resonance without also strongly amplifying low-frequency disturbances. The results are summarized in Table I, which shows the results numerically in terms of the RMS of $\ddot{x}_2$.

The position of the isolated mass x_2 is used as a performance indicator when evaluating feedforward since position feedforward was implemented. To show the influence of feedforward on the reduction of indirect disturbances, only these were used to excite the system. In Fig. 3b the

obtained CPS are plotted. While the feedback control, to a large extent, removes the amplification of vibration due to the resonance, it does not influence the low-frequency vibration transmission. When feedforward is used, the low-frequency contributions are reduced, which results in an almost 95% decrease in the final vibration magnitude. This shows that even straightforward stiffness compensation feedforward can greatly improve systems performance. These results can be found numerically in Table II.

IV. Conclusion

This paper investigated the use of ultra hard mounts based on piezoelectric stack actuators in applications requiring high position stability. Thanks to the high stiffness of the actuators and the application of active damping for resonance peak reduction, the influence of direct disturbance forces on such a system is greatly diminished. Even though the system is characterized by high resonance frequency, the transmissibility of the base vibrations is reduced with the feedforward techniques.

The performance of feedback and feedforward techniques, developed for other systems and utilizing various sensor types, was evaluated by implementing them on a high stiffness single-degree-of-freedom experimental test setup.

It was found that high degrees of damping can be achieved with acceleration based feedback controllers. The amount of damping is limited by amplification of disturbances, and excitation of high frequency modes. At the cost of more elaborate tuning NAF and VBP outperform VFB. If absolute position measurements are available PPF can be used for performance approaching that of VFB. However, the in practice easier to obtain, relative position measurement cannot reach similar damping. To solve the indirect disturbance sensitivity drawback of ultra hard mount systems, feedforward was implemented. It was shown that even with straightforward stiffness compensation feedforward, the transmissibility can be lowered significantly. The outcomes of the study motivate further research on the concept of ultra hard mounts.

References

[1] D. Tjepkema, J. Van Dijk, and H. M.J.R. Soemers. "Sensor fusion for active vibration isolation in precision equipment". In: *Journal of Sound and Vibration* 331 (4 Feb. 2012), pp. 735–749. ISSN: 0022-460X.

[2] Christophe Collette, Stef Janssens, and Kurt Artoos. "Review of active vibration isolation strategies". In: *Recent patents on Mechanical engineering* 4.3 (2011), pp. 212–219.

[3] Tjeerd van der Poel et al. "Improving the vibration isolation performance of hard mounts for precision equipment". In: *2007 IEEE/ASME international conference on advanced intelligent mechatronics*. IEEE. 2007, pp. 1–5.

[4] Shingo Ito and Georg Schitter. "Comparison and classification of high-precision actuators based on stiffness influencing vibration isolation". In: *IEEE/ASME Transactions on Mechatronics* 21.2 (2015), pp. 1169–1178.

[5] PI PI Ceramic GmbH. *Properties of Piezo Actuators — piceramic.com*. [Accessed 30-03-2024].

[6] Mark J Balas. "Direct velocity feedback control of large space structures". In: *Journal of guidance and control* 2.3 (1979), pp. 252–253.

[7] André Preumont et al. "Force feedback versus acceleration feedback in active vibration isolation". In: *Journal of sound and vibration* 257.4 (2002), pp. 605–613.

[8] C J Goht and T K Caugheys. "On the stability problem caused by finite actuator dynamics in the collocated control of large space structures". In: *Taylor and Francis* 41 (3 1985), pp. 787–802. ISSN: 1366-5820.

[9] MA Beijen et al. "H∞ feedback and feedforward controller design for active vibration isolators". In: *IFAC-papersonline* 50.1 (2017), pp. 13384–13389.

[10] L. van de Ridder et al. "Coriolis mass-flow meter with integrated multi-DOF active vibration isolation". In: *Mechatronics* 36 (June 2016), pp. 167–179. ISSN: 0957-4158.

[11] W. B.J. Hakvoort, G. J. Boerrigter, and M. A. Beijen. "Active vibration isolation by model reference adaptive control". In: vol. 53. Elsevier B.V., 2020, pp. 9144–9149.

[12] Colin G Gordon. "Generic vibration criteria for vibration-sensitive equipment". In: *Optomechanical Engineering and Vibration Control*. Vol. 3786. SPIE. 1999, pp. 22–33.

[13] L Jabben and J Van Eijk. "Performance analysis and design of mechatronic systems". In: *Mikroniek* 51.2 (2011), pp. 5–12.

[14] Sang-Myeong Kim, Semyung Wang, and Michael J Brennan. "Comparison of negative and positive position feedback control of a flexible structure". In: *Smart Materials and Structures* 20.1 (2010), p. 015011.

[15] Marcin B Kaczmarek and Hassan HosseinNia. "Fractional-Order Negative Position Feedback for Vibration Attenuation". In: *Fractal and Fractional* 7.3 (2023), p. 222.

[16] Gabriele Cazzulani et al. "Negative derivative feedback for vibration control of flexible structures". In: *Smart Materials and Structures* 21.7 (2012), p. 075024.

[17] Hassaan Hussain Syed. "Comparative study between positive position feedback and negative derivative feedback for vibration control of a flexible arm featuring piezoelectric actuator". In: *International Journal of Advanced Robotic Systems* 14.4 (2017), p. 1729881417718801.

[18] Ahmad Paknejad et al. "A novel design of positive position feedback controller based on maximum damping and H2 optimization". In: *Journal of Vibration and Control* 26.15-16 (2020), pp. 1155–1164.

[19] Guoying Zhao et al. "Nonlinear positive position feedback control for mitigation of nonlinear vibrations". In: *Mechanical systems and signal processing* 132 (2019), pp. 457–470.

3

Experimental Results

This chapter expands upon the results presented in the paper above. In the first section, 3.1 details regarding the experimental setup are given, the controllers used in the research are recited and more information on the performance measure is given. In the next section, 3.2, the simulation model that was created to test different approaches and predict their damping performance is discussed and its dynamics are compared to the experimental setup in open and closed loop. In section 3.3, the influence and choice of controller gain on the performance is discussed. Next, in section 3.4 the results presented in the paper above are discussed in more depth. Finally, in section 3.5 the disturbance feedforward control method introduced in the paper is derived in more detail and elaborated upon.

3.1. Experimental Setup

In this section some details on the experimental setup are repeated from the paper in more depth. The experimental setup is presented, the feedback methods that have been introduced in the paper are repeated and the performance definition is given.

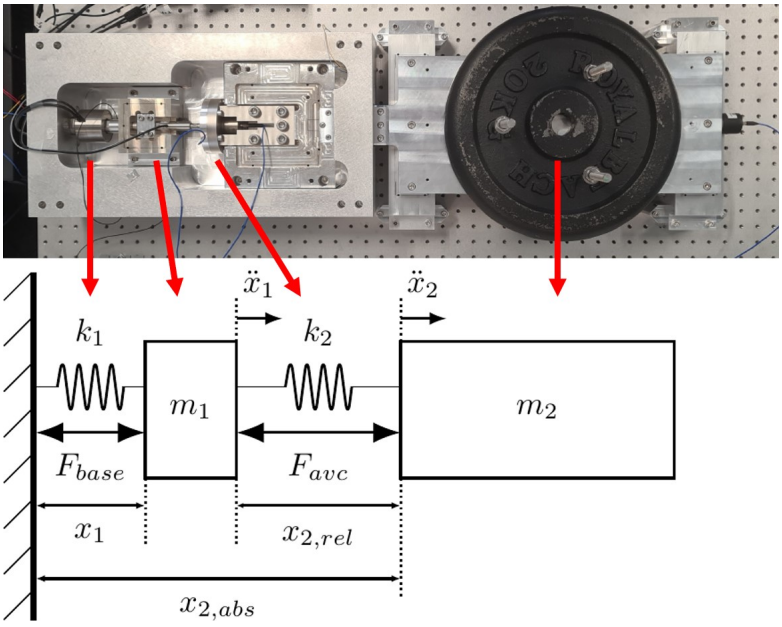

Figure 3.1: Top-down view of the experimental setup with corresponding mass-spring model. The mass m_2 represents sensitive equipment that is to be isolated with vibration control. This mass can be varied to change the resonance frequency. The base piezo-stack actuator F_{base} is used to control the mass representing the floor m_1 to introduce an indirect disturbance. The other piezo-stack actuator F_{avc} is used both to excite the system with a direct disturbance and to apply active vibration control.

A single-axis experimental setup, shown in figure 3.1, is used to represent an ultra hard mount system. A platform with adjustable mass represents the payload to be supported, indicated by m_2. This mass was chosen at 56kg such that the resonance frequency was 103Hz. By choosing a lower mass the frequency may be shifted to a higher frequency. The motion of m_2: x_2 and $\ddot{x}_2$, will be referred to as the output of the vibration isolation system. The main stack actuator, indicated by F_{avc} constitutes the ultra hard mount and connects the payload to the shaking base, m_1. This shaking base is actuated by another stack actuator indicated by F_{base}. Motion of all elements of the setup is constrained to a single degree of freedom using flexures. More details regarding the experimental setup are provided in Appendix A.

The feedback controllers under investigation are described in more detail in the paper. The three acceleration-based controllers analyzed are: Velocity Feedback (VFB), Velocity Bandpass Feedback (VBP), and Negative Acceleration Feedback (NAF). Additionally, the two displacement-based control methods for investigating different sensing options are: Relative Positive Position Feedback (rel. PPF) and Absolute Positive Position Feedback (abs. PPF).

As explained in the paper the performance of the system is defined in terms of the root-mean-square (rms) of the output vibration (i.e. the motion of isolated mass m_2). The system was excited with an indirect and direct disturbance (shown in figure 1.1a) and the acceleration or displacement of the isolated mass was measured. From these measurements the Power Spectrum Density (PSD) was calculated. This has been integrated to create a Cumulative Power Spectrum (CPS), according to the Dynamic Error Budgeting (DEB) method introduced in [20]. The CPS visualizes the contribution to the total error at each frequency, and the final value of the CPS represents the total error. These CPS plots are provided in the paper and the coming sections to show the performance. The DEB method is described in more detail in Appendix D.

3.2. Predicting Damping with Simulations

This section discusses the use of a simulation model to predict the closed loop damping behaviour of the experimental setup. A simplified model was created in Simulink using the Simscape package. The system was modelled as the double mass-spring system as shown in 3.1. As such the model disregards high-frequency internal dynamics. The sensor gains in the model were set such that the magnitude of the transfer functions between control signal and outputs match between model and experimental setup. In figure 3.2a Bode plots of the responses of the Simscape model and experimental setup are compared. The simulated and measured transfer functions from control signal, v, to the displacement of the isolated mass x_2 are plotted. Likewise, the transfer functions from v to the acceleration of the isolated mass a_2 ($\ddot{x}_2$) are shown. The transfer functions match well below and around the resonance frequency at 103 Hz. However, the high frequency modes at 1100 Hz are not modelled, and as such the model and measurements deviate quite a lot above 450 Hz. For the investigation of damping performance of the methods this region is not of interest as these modes do not directly influence the damping behaviour. Therefore, below and around the resonance frequency the assumption that the setup can be described as a double mass-spring system holds. Furthermore, it can be seen that the setup suffers from delay. The modelled delay of 0.5 ms matches the delay of the setup. This delay can be attributed to the long signal path from control signal to measurement, and updating loop within the data acquisition device. This is discussed in more detail in Appendix A. In figure 3.2b the transmissibility from x_1 to x_2 is plotted up to 350 Hz. It can be seen that the transmissibility of the model and experimental setup match well.

The model was used to predict the damping with different controllers, the results can be seen in Figure 3.3. For each approach the open loop Transmissibility has been plotted in dotted blue, the simulated closed loop response in orange and the measured closed loop transmissibility in yellow. Due to the simplified nature of the model, it doesn't capture all the dynamics of the system. Noticeably, there is a mode at around 200 Hz, that influences the behaviour around the resonance. In the system this leads to a less smooth profile than the predicted model response. However, the model is able to predict the overall damping performance well.

The high frequency modes, visible in figure 3.2a, may not be influential to the damping of the system but they are important factors for the performance of the system. Controller gain at this frequency will excite these modes. The result is an increased contribution to the total error, visible in the cumulative

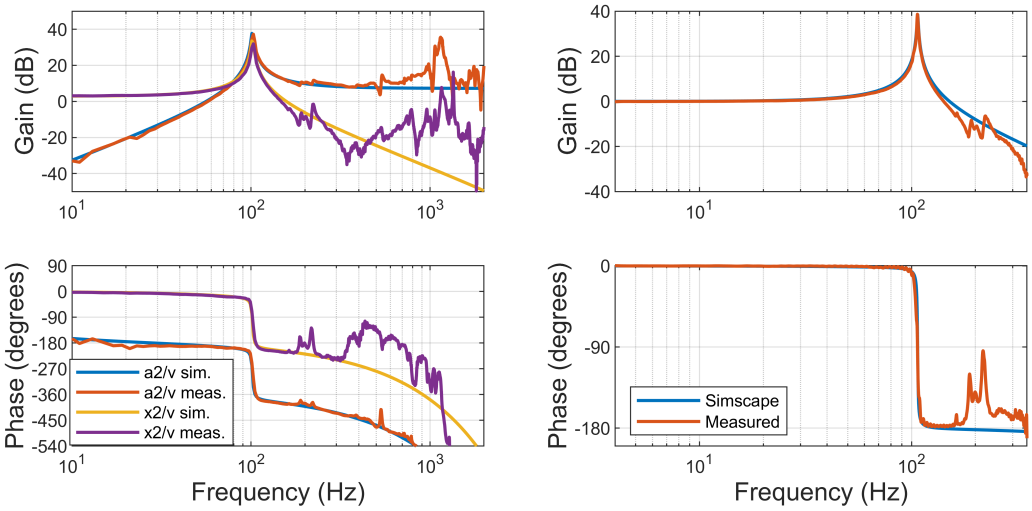

(a) Comparison between model and experimental setup response from AVC control signal v to the position x_2 and acceleration a_2 of the isolated mass.

(b) Comparison between the between simulated and calculated transmissibility from x_1 to x_2.

Figure 3.2: Comparison between simulated model response and measured experimental setup response. It can be seen that the response from control signal to output match well between the simulation and experimental setup until 350 Hz.

power spectra shown in the next sections. Another consequence is a decreased stability margin, that will be explored more in depth in the next section.

The tuning of the controllers shown in this section is based on the findings of the next section which explores the influence of controller gain.

3.3. Influence of Controller Gain

This section discusses the influence of controller gain on the performance in terms of output vibration levels. Tuning of the controller parameters was done with rules found in literature, as described in the paper above. However, in literature the optimal gain is determined by optimizing for a single transfer function. In the presence of multiple disturbance sources (floor, force and electronic noise), these optima do not hold. Furthermore, high frequency modes that are not modelled strongly limit the controller gain. Therefore, the controller gain is determined experimentally. In this chapter the influence of controller gain on vibration control performance is discussed using two examples: Velocity Feedback, based on acceleration measurements, and Absolute Positive Position Feedback, based on displacement measurements.

In figure 3.4, the influence of gain on Velocity Feedback is explored. This controller is based on integration of acceleration measurements and has the desired triangular open loop gain shape as can be seen in figure 3.4a. The influence of open loop gain shape is discussed in the paper, the triangular shape prevents noise amplification and influence on the dynamics at frequencies other than the resonance frequency. Increasing the controller gain shifts the entire open-loop response to a higher magnitude. The resulting higher open-loop gain around the resonance frequency leads to higher damping. However, this same increase leads to increased noise and disturbance amplification. Furthermore, it can also be seen that the modes at 1000 Hz are shifted closer to the 0 dB line. This decreases the stability margin that is determined by the distance between these modes and the 0 dB line. In turn leading to an increased amplification of noise at this frequency. Instability follows if the modes come too close or cross this line due to too much controller gain.
In figure 3.4b, the impact of controller gain on the output vibrations can be found. The response of the passive structure, plotted in dotted blue, is marked by a sharp increase at 100 Hz from its resonance peak. This resonance is well damped with the use of Velocity Feedback, evident from the smaller increase at 100 Hz. An increase in gain leads to more damping. However, it also leads to an increase in error below the resonance due to amplification of disturbances by the controller. It can be seen that if the

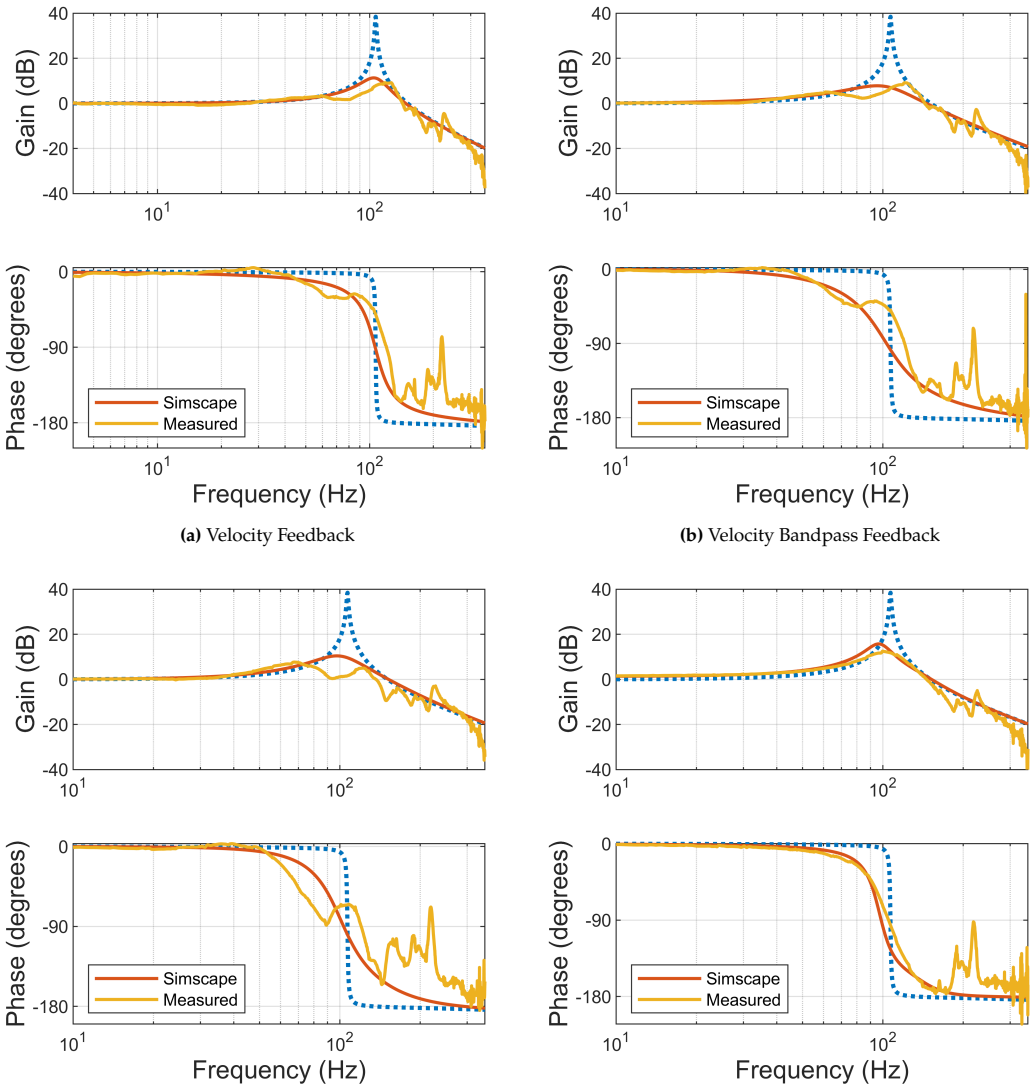

(a) Velocity Feedback

(b) Velocity Bandpass Feedback

(c) Negative Acceleration Feedback

(d) Absolute Positive Position Feedback

Figure 3.3: Closed loop response of the Simscape simulation model compared to the measured closed loop response of the experimental setup with different AVC feedback methods

gain is too high this amplification effect is larger than the reduction at 100 Hz by the added damping. Subsequently the total performance decreases. Finally, the effect of reduced stability margins can be seen at around 1000 Hz. Increased gain leads to excitation of these modes, resulting in an increase in the total error. There is a trade-off between damping and noise amplification.

The other acceleration-based controllers, Velocity Bandpass Feedback and Negative Acceleration Feedback, were designed to create a 'sharper' triangular shape. The motivation behind this is that for the same gain at the resonance frequency there is less amplification at other frequencies. Alternatively, the gain at the resonance frequency can be increased, with the same amount of noise amplification. Although their open-loop shape is improved, these controllers have the same trade-off between damping and disturbance amplification.

The displacement-based controllers do not have the desired triangular open loop gain shape. The open-loop gain for Positive Position Feedback with different controller gains can be found in figure 3.5a. Instead of a triangular shape, positive position feedback controllers have high gain at low frequencies. This leads to stronger amplification of low frequency disturbances, compared to a more optimal pyramid open loop shape. This can be seen in the CPS plot in figure 3.5b, where the error at low frequencies is

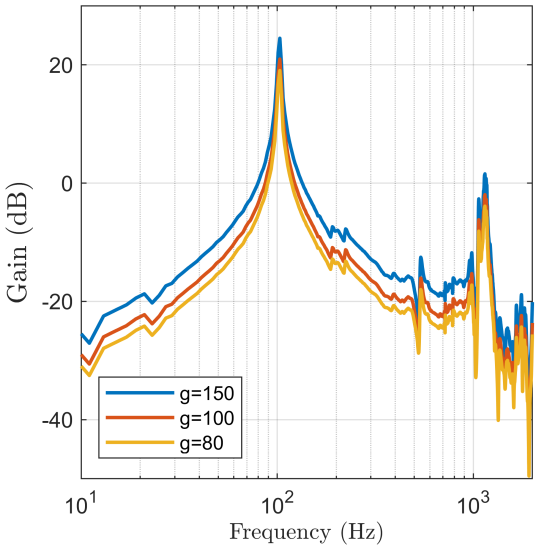

(a) Open-Loop of Velocity Feedback with different controller gains showing an increase in response with an increase in controller gain.

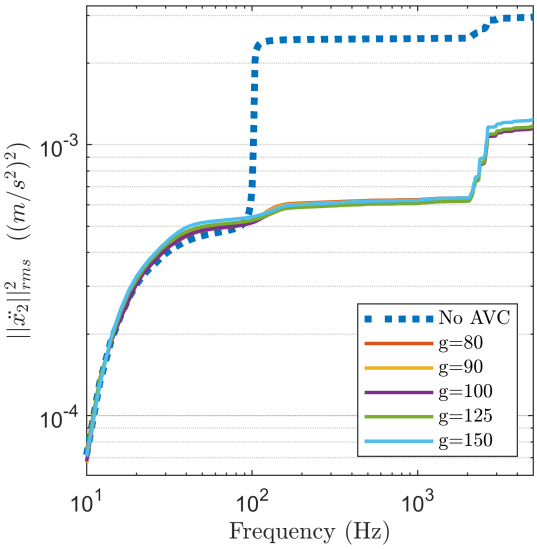

(b) CPS results with different controller gains, showing that an increase in controller gain leads to increased damping, but also an increase in noise amplification and increased excitation of high-frequency modes.

Figure 3.4: The influence of gain on the open-loop gain and cumulative power spectrum using Velocity Feedback using acceleration measurements.

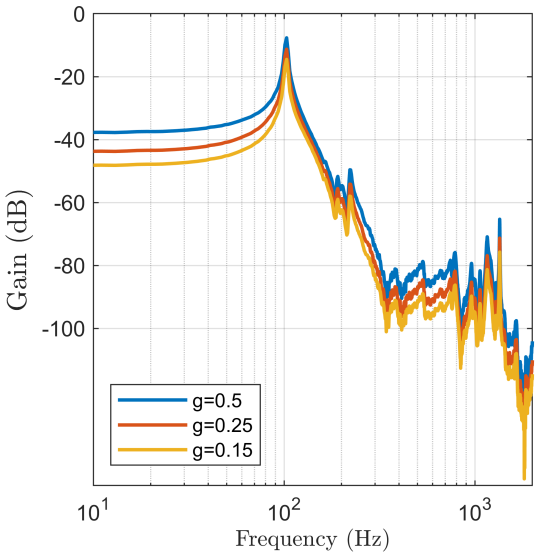

(a) Open-Loop of Positive Position Feedback with different controller gains. PPF controllers do not have the desired triangular open loop shape.

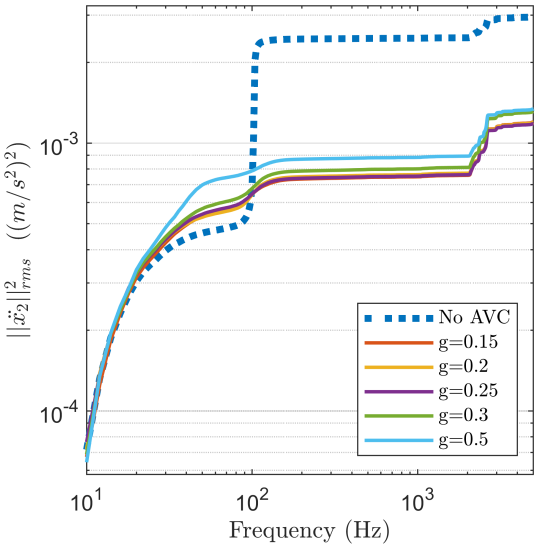

(b) CPS results with different controller gains, showing that an increase in controller gain leads to increased damping. However, due to the open-loop shape the low frequency noise amplification effect is strong, limiting the performance.

Figure 3.5: The influence of gain on the open-loop gain and cumulative power spectrum using Positive Position Feedback with absolute displacement measurements

much higher compared to the open-loop response. For higher controller gains this effect is emphasized, strongly limiting the possible damping.

The best controller gain was found by performing these gain sweeps, and choosing the gain for which the total error was lowest. This was done for each method. The open loop gain of each controller with the resulting gain can be found in figure 3.6a. In figure 3.6b, the measured transmissibility of each feedback approach is plotted for comparison. As expected the maximum damping of the positive position

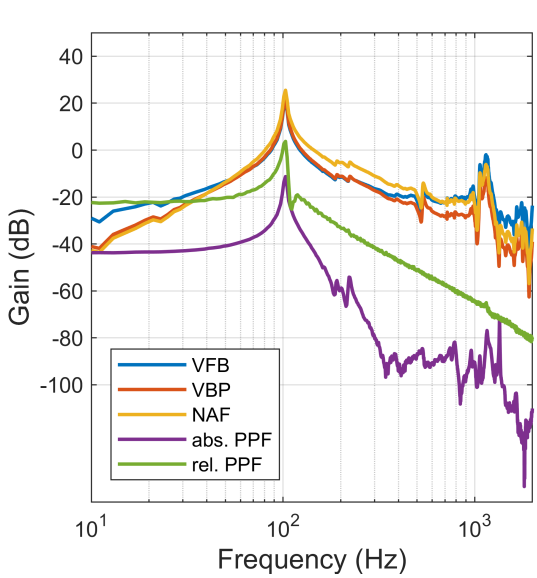

(a) Open-Loop gain of the different feedback controllers. The acceleration-based controllers have a better open-loop shape than the displacement-based controllers.

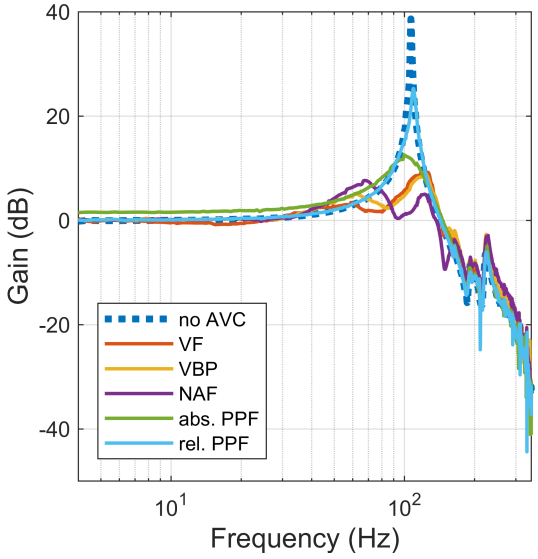

(b) Transmissibility with different feedback controllers. The acceleration-based controllers add more damping than the displacement-based controllers. Absolute PPF has a softening effect on the system resulting in an increase in transmissibility at low frequency.

Figure 3.6: Open-loop gains and transmissibilities of the different feedback methods with the controller gains found with the gain sweeps.

feedback methods is lower than the possible damping of the acceleration-based methods. Absolute Positive Position Feedback has a softening effect, which results in an increased transmissibility response before the resonance frequency limiting the amount of damping. Also noticeable is that the amount of damping is less than the critical amount of damping. This is due to this trade-off behaviour between the amplification of noise and disturbances by the controllers. The gain sweeps for each controller can be found in Appendix B.

3.4. Feedback Results

In this section the experimental results with the different feedback controllers are presented. These results were also presented in the paper. Figure 3.7a shows the Cumulative Power Spectrum of the system without and with active vibration control. Without control the major contributions to the total error are caused by the resonance peak at 103 Hz and the high-frequency modes at 1100Hz. With active damping, the contribution of the resonance peak is reduced significantly.

Especially the acceleration-based control methods, Velocity Feedback (VFB), Velocity Bandpass Feedback (VBP), and Negative Acceleration Feedback (NAF), achieve very high degrees of damping, showing only a small increase at 103Hz. However, visible from the increase before the resonance frequency compared to the open-loop, noise is amplified by all controllers. Furthermore, the high-frequency parasitic modes at around 1100 Hz are excited by the controllers, leading to an increase in vibrations.

The performance of Positive Position Feedback using absolute position measurements approaches the performance of velocity feedback even though the possible amount of damping is lower due to the amplification of the base-vibration. This is thanks to smaller excitation of the high-frequency dynamics.

Relative Positive Position Feedback is not able to achieve similar performance, due the shape of the open-loop gain (visible in figure 3.6a). It can be seen that relative PPF has high open-loop gain at low frequencies without a significant peak at the resonance frequency. As a result, it is not possible to dampen the resonance without also strongly amplifying low-frequency disturbances.

A brief investigation was performed with a different disturbance case, which can be found in Appendix C. To test the a floor disturbance dominant case, the indirect disturbances were increased with a smaller force disturbance. It was found that the relative performance between feedback methods did not change.

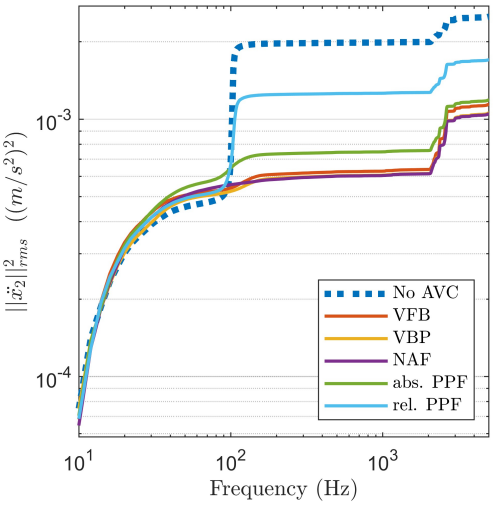

(a) Cumulative power spectrum of $\ddot{x}_2$ showing the system response to direct and indirect disturbance excitation without AVC and with different feedback strategies implemented.

Method	RMS of $\ddot{x}_2$ (m/s^2)	% of No AVC
No AVC	2.50×10^{-3}	100%
VF	1.14×10^{-3}	45.7%
VBP	1.06×10^{-3}	42.3%
NAF	1.05×10^{-3}	41.9%
abs. PPF	1.19×10^{-3}	47.5%
rel. PPF	1.70×10^{-3}	68.1%

(b) Numerical results of experimental evaluation of different AVC feedback strategies showing the RMS of the acceleration of the isolated mass $\ddot{x}_2$ of each strategy and the percentage with respect to no AVC.

Figure 3.7: Experimental results of the different feedback methods. The system was excited with direct and indirect disturbances and the output vibrations were measured. This was done without AVC control and with the different feedback methods. In the CPS it can be seen that with feedback the vibration levels are decreased due to the damping of the resonance peak.

Acceleration-based controllers outperformed the displacement-based controllers in the same way as the situation described above. Similar performance gains could be made with more elaborate tuning of Velocity Bandpass and Negative Acceleration Feedback compared to Velocity Feedback.

3.5. Disturbance Feedforward on Ultra Hard Mount

This section discusses the effect of feedback on the transmissibility and using feedforward to lower the transmissibility. As mentioned before, a big drawback of using high stiffness mounts is the wide frequency range for which the transmissibility equals 1. It can be seen in the sections above that the feedback methods do not lower the transmissibility outside reducing the resonance peak by adding damping. However, one way to use feedback to lower the transmissibility is to add 'virtual mass' to the system. This is done by adding gain directly to an acceleration measurement in feedback, mimicking the effect of adding physical mass to the system, combined with velocity feedback for damping. $K_{vm} = \frac{g_m s + g_d}{s+\omega_i} \frac{\omega_{lp}}{s+\omega_{lp}}$. The controller has a virtual mass gain g_m and a gain for damping g_d. The low-pass is used to reduce the high frequency gain and its corner frequency is set just after the resonance peak. This approach is illustrated in Figure 3.8. In figure 3.8a it can be seen that by adding virtual mass feedback the resonance peak can be shifted to a lower frequency. However, figure 3.8b shows that even in combination with a low pass filter, adding virtual mass leads to excessive excitation of high frequency modes and amplification of noise. This drastically reduces the stability margins of the system (to the point of instability), while decreasing the transmissibility only slightly.

A more robust and effective method of lowering the transmissibility is to use disturbance feedforward control. In the rest of this section, this method is introduced, and a straightforward stiffness compensation controller is derived, and implemented.

A block diagram representation of an active vibration control system with feedback and feedforward controllers is shown in figure 3.9. The approach of feedforward is to measure the incoming indirect disturbance and create a control signal to cancel its influence on the output. Since $x_2 = P_1 \cdot x_1 + C_{ff} \cdot K_{ff} \cdot P_2 \cdot x_1$, x_2 equals zero if: $P_1 = -C_{ff} \cdot K_{ff} \cdot P_2$. If sensor dynamics are ignored, perfect cancellation occurs when $K_{ff} = -P_1/P_2$. Working this out results in $K_{ff} = -(k + c \cdot s)$, with stiffness k and damping c, for a simple 1 degree of freedom mass-spring-damper system.

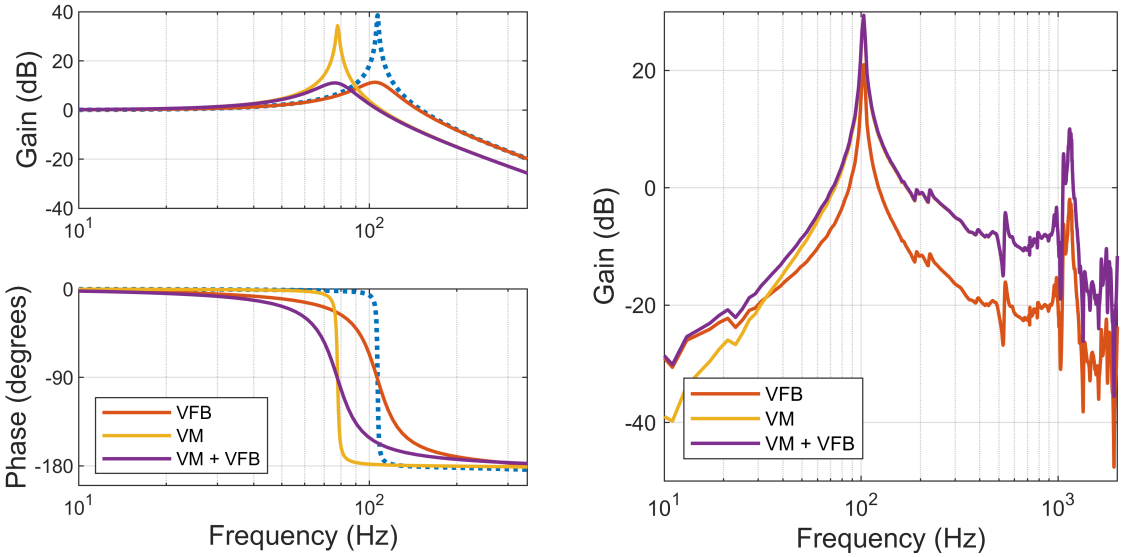

(a) Transmissibility with Velocity Feedback (VM), Virtual Mass feedback (VM), and Velocity with Virtual Mass feedback (VM+VF)

(b) Open loop gains of Velocity Feedback (VM), Virtual Mass feedback (VM), and Velocity with Virtual Mass feedback (VM+VF)

Figure 3.8: Reducing the transmissibility using Virtual Mass Feedback. Virtual Mass Feedback uses measurements of the acceleration of the isolated mass to mimick the effect of adding physical mass to the system, lowering the resonance frequency. Even though a low-pass filter is used to reduce high frequency gain, the open-loop gain is still increased significantly for a small reduction in transmissibility.

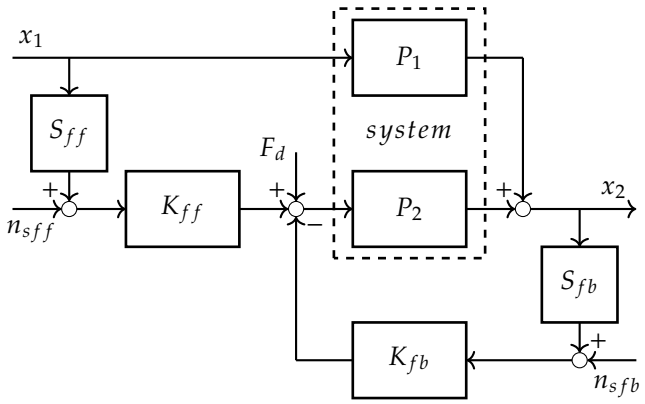

Figure 3.9: Block diagram representation of an active vibration control system with both feedback and feedforward. Transfer function P_1 and P_2 represent the transmissibility and compliance respectively. S_{ff} and S_{fb} are the sensor dynamics for the feedforward and feedback controllers K_{ff} and K_{fb}. The sensors add noise n_{sff} and n_{sfb} to the system. F_d and x_1 denote the direct and indirect disturbances.

In practice estimates for k and c will never be perfect because of identification errors, non-linearities, and time-varying effects. Moreover, it is not always possible to excite the floor sufficiently for proper identification. For this reason often self-tuning filters are used to reach higher performance [23, 24].

If the stiffness of the system is known, or the transmissibility and compliance can be well identified, the most straightforward disturbance feedforward method is stiffness compensation. With this method only the stiffness is accounted for: $K_{ff} = -k$. Feedforward is often used in combination with feedback, which is used to add damping to the system.

In figure 3.10a the simulated influence of disturbance feedforward on the transmissibility can be found. The pure stiffness compensator feedforward controller $K_{ff} = -k$ is plotted as "FF no filters". It can be seen that the entire transmissibility response is decreased by 20 dB. However, as shown in 3.10b, the actual measured transmissibility does not match. After about 200 Hz the effects of the delay become so large that feedforward is not effective any more. As a result the transmissibility is not lowered.

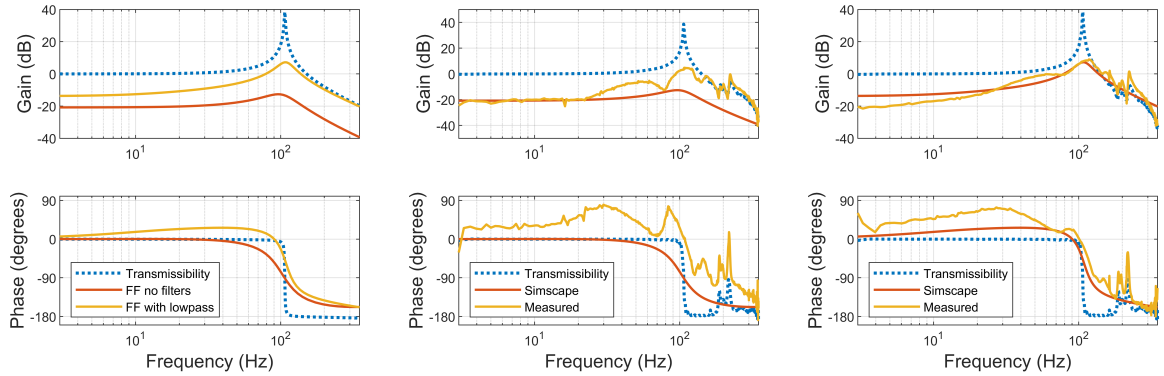

(a) Simulated feedforward and influence of low-pass filter

(b) Simulated vs measured response without low-pass filter

(c) Simulated vs measured response with low-pass filter

Figure 3.10: Disturbance feedforward can be used to lower the transmissibility over a wide frequency range. However, the theoretically possible performance is not possible in practice due to unmodelled system dynamics and delays. To counteract high frequency excitation by the feedforward controller caused by delays a low-pass filter is added to the stiffness compensation controller. This reduces the effect on the transmissibility but makes the controller more predicable.

Moreover, this behaviour results in added noise to the system. To counteract this, a low pass can be added to the system. In figure 3.10a it can be seen that this decreases the effect of feedforward on the transmissibility. Figure 3.10c shows that with an added low-pass the simulated and measured response match well. Sources of delay are discussed in Appendix A. The total delay was measured to be about 500 microseconds.

With a low-pass filter the feedforward controller becomes:

$$K_{ff} = -k \frac{\omega_{lp}}{s + \omega_{lp}}.$$

It was found that ω_{lp} set at 150 Hz provided good results. This prevented the unwanted high frequency behaviour.

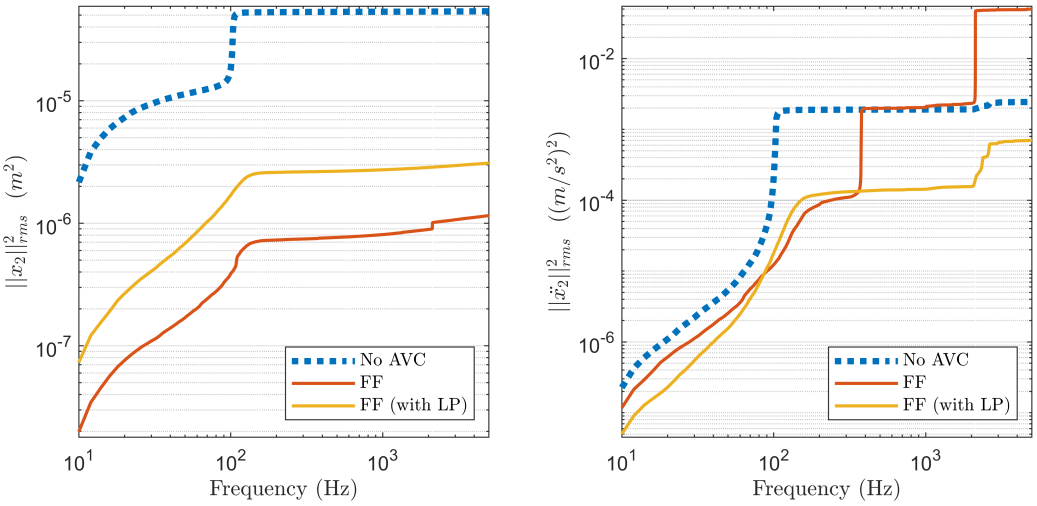

(a) CPS with x_2 as performance indicator, showing the decrease in effect on the transmissibility when including a low-pass (LP) filter.

(b) CPS with $\ddot{x}_2$ as performance indicator, showing the excitation of high-frequency dynamics of feedforward without low-pass (LP) filter due to delays.

Figure 3.11: Adding a low-pass filter to feedforward results reduction of the effect the controller has on the transmissibility. This visible decrease in performance is shown when measuring the output displacement. However, the high-frequency excitation of the system visible when measuring acceleration is apparent showing the need for the filter.

Figure 3.11 shows the effect of adding a low-pass filter to the feedforward controller on the output vibration levels. The system was excited with only indirect disturbances to show the influence of feedforward on indirect disturbance rejection. Figure 3.10a shows that this is expected as the transmissibility is lowered less with low-pass filter. Figure 3.11b shows the output performance in terms of $\ddot{x}_2$. The benefit of adding a low-pass filter can be seen clearly. Without the filter all modes above 200 Hz are excited excessively, resulting in a twentyfold increase in acceleration of the output.

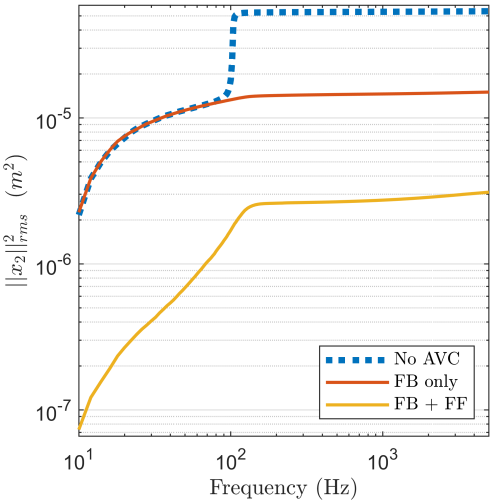

(a) CPS with x_2 as performance indicator showing the influence of feedback and feedforward.

Method	RMS of x_2 (m)	% of No AVC
No AVC	5.38×10^{-5}	100%
FB	1.50×10^{-5}	27.9%
FB + FF(LP)	3.10×10^{-6}	5.8%

(b) Numerical results of experimental evaluation of indirect disturbance rejection with feedback and with feedforward with low-pass (LP) filter showing the RMS of the position x_2 of the isolated mass and the percentages with respect to no AVC.

Figure 3.12: Experimental results of feedback and feedforward with only floor disturbance. The effect of feedback on the transmissibility is damping of the resonance peak. This results in a lack of increase at the resonance frequency. However, below the resonance frequency the contribution to the error is equal with open loop, as feedback does not reduce the transmissibility below the resonance frequency. Feedforward does reduce the transmissibility over a wide frequency range, resulting in a much lower error.

In figure 3.12, the results of feedforward can be found compared to using only feedback. It can be seen that feedback is able to dampen the response of the system, reducing the rms of the output displacement to 27.9%. However, below the resonance frequency the increase in error is equal to no control, as the transmissibility equals 1 until this frequency. Using disturbance feedforward (with low-pass) the transmissibility is reduced and as such the total error. The rms of the displacement of the isolated mass is reduced to 5.8% compared to open loop. This is a reduction of more than 22% compared to only feedback. These results show that with feedforward the sensitivity of ultra hard mount systems to floor vibrations may be reduced significantly.

4

Conclusion and Recommendations

In this final chapter conclusions will be drawn and recommendation for future work are provided. Some of the conclusions have already been provided in the paper but are repeated here in more depth. In section 4.1 the work is summarized, the key results are interpreted and conclusions are provided. In section 4.2 recommendations regarding future research topics that may build on this work are given.

4.1. Conclusions

This work aimed to explore the feasibility of using very high stiffness system mounting as a solution for guaranteeing position stability in the presence of substantial direct disturbances. These ultra hard mount systems are characterised by superior direct disturbance rejection at the cost of elevated susceptibility to indirect disturbances. Active vibration control has previously been used successfully to improve the performance of hard mount systems but remained largely unexplored on ultra hard mounts. In order to investigate the viability of using ultra hard mount systems in the context of vibration control, the following two research objectives were set:

- *Experimentally analyse and compare the influence of different active vibration control techniques on the performance of an ultra hard mount system.*
- *Investigate the feasibility of disturbance feedforward on an ultra hard mount system as a way to lower its sensitivity to indirect disturbances.*

Experimental analysis was performed on a piezo-based single degree of freedom setup. An important transfer function of ultra hard mount systems is the transmissibility, which describes how indirect disturbances influence the output. The transmissibility of ultra hard mount systems are characterized by a high resonance frequency. The transmissibility of the different active vibration control feedback methods was simulated and compared against the response of the structure and the measured response. It was found that damping can be predicted well with a simplified representation of the experimental setup, showing that the behaviour of piezo-based systems can be predicted well. Some dynamics not included in the simulation model influenced the behaviour around the resonance frequency. However, the amount of damping and overall closed loop behaviour can be modelled accurately. Due to unmodelled high frequency modes, the simulation model is only accurate up to around 450 Hz, showing the benefit of experimental testing and evaluation.

The influence of controller gain on the performance was evaluated by exciting the structure with indirect and direct disturbances and measuring the total error with different controller gains. It was found that increasing the gain leads to a trade-off between more damping and excitation of high-frequency modes and the amplification of noise. This put strong limits on the total performance. The maximum damping is dependent on the dynamics of the disturbance signals. Due to this dependency, the specific limits may vary between applications. Higher levels damping can be reached in applications with smaller disturbances.

It was found that the open loop dynamics of Velocity Feedback can be improved by reducing controller gain at frequencies other than the resonance frequency through more elaborate controller design. As a result, Velocity Bandpass Feedback and Negative Acceleration Feedback outperform velocity feedback due to lower noise amplification. The displacement-based controllers are not able to reach similar damping due to their open loop shape, that results in amplification of low frequency noise. However, Absolute Positive Position Feedback approached the performance of Velocity Feedback due to the lower excitation of high-frequency modes, despite the lower level of damping. The in practice easier to obtain Relative Positive Position Feedback is not able to achieve similar performance, due to its bad open loop shape.

Although the total vibration levels can be reduced significantly with feedback due to damping, the transmissibility of indirect disturbances remains high. It was found that feedforward can considerably reduce the effect indirect disturbances have on the output. However, due to delays in the system and sensor dynamics the theoretically possible reduction was not met. A low-pass filter can negate the negative effect of these delays. With straightforward stiffness compensation feedforward a reduction in output vibration levels of about 94% is reached. This shows that feedforward can be used to solve the main drawback of ultra hard mount systems.

To conclude, ultra hard mount platforms offer superior direct disturbance rejection over less stiff systems. Piezoelectric transducers are a good solution to make such a system active, having high stiffness and offering precise and predictable controllability. The closed loop behaviour of such a system can be modelled accurately. The resonance mode may be damped significantly but the total damping is limited by noise amplification from increased control effort. The main weakness of an ultra hard mount system is its high resonance frequency resulting in increased susceptibility to indirect disturbances. It was shown that this weakness may be overcome with disturbance feedforward.

A combined feedforward and feedback approach can be used to enable the use of ultra hard mount systems in applications where the present indirect disturbance sources would disqualify a passive structure of the same stiffness. This opens up new possibilities for systems were position stability in the presence of high force disturbances has to be guaranteed but ultra stiff mounts were previously not an option.

4.2. Recommendations

The findings of this research show that active vibration control can be used to improve the performance of ultra hard mount systems and decrease the sensitivity to floor vibrations. This motivates further research on the topic of ultra stiff active vibration control systems. In this chapter some recommendations are given for topics to explore next in no particular order.

Optimization of the various feedback controllers is not something this research has focused on but is interesting to explore. The Dynamic Error Budgeting method that has been employed for evaluation can also be used as a design tool. If an accurate model of the system can be created and the disturbances for a specific application are known intimately, this method can be used to predict the performance. Consequently, optimization techniques could be used to find optimal tuning for specific disturbance cases. This was attempted but it was found that the model used could not accurately describe the behaviour of the high-frequency modes. As such it could not accurately predict the total vibration levels of the isolated mass. In appendix D this trial has been described in some more detail. If optimization is of primary concern, than work can be done to make this model more accurate, and use it for optimization.

However, the biggest performance gains were not made with feedback but with disturbance feedforward. Due to the high resonance frequency, ultra hard mounts are susceptible to a wide frequency band of indirect disturbances. As a consequence, they can either be used only in very quiet environments, or disturbance feedforward needs to be able to reduce the floor vibrations to acceptable levels. It was shown that with straightforward stiffness compensation the transmissibility can be lowered. Work can be done to improve the performance further with more elaborate feedforward. Although there is not much disturbance feedforward research done on ultra hard mount system, there has been quite a lot work done on hard mount systems [10, 19, 25]. These state of the art techniques can be adapted to ultra hard mount systems.

Additionally, the current setup suffers from delays that limit the bandwidth of the feedforward controller. These delays are largely caused by conversions from digital to analog due to the use of Labview. Work can be done in lowering these delays to push the bandwidth of the feedforward controller, and increase the effective frequency range. This would require a redesign of the electronic side of the experimental setup. However, it would result in an improvement in performance with the current stiffness compensation controller without the need for complex filtering and parameter estimation.

This work has been done in a single degree of freedom. In real world application this assumption does not hold. Real floor vibrations may have rotational components. Direct disturbances will also be much more complex than single degree of freedom forces directly in line with the active vibration control actuator. It will be interesting to extend these results to multiple degrees of freedom. Multi-axis disturbance feedback and feedforward control has been investigated previously but not on ultra stiff piezo-based systems [19, 26, 27, 28].

Hysteresis is a known factor to influence the behaviour and performance of piezo-based systems. This work has not investigated the influence of this phenomenon in the context of vibration control. However, to increase understanding of piezo-based systems for active vibration control, the effect of hysteresis on damping and disturbance feedforward is of interest.

Lastly, for this research two disturbance profiles were chosen to represent a typical application case. Floor vibrations were based on the VC-C curve [6] and a representative force disturbance was provided by PI. The experimental results showed a that the maximum damping levels were dependent on amplification of noise and disturbances. Therefore, the performance limits may be different for other disturbances cases. This has been briefly investigated in Appendix C. It was found that the feedback results were very similar to case used in this thesis. However, it may be interesting to further investigate the performance with different disturbance cases or disturbances with different dynamics.

References

[1] Butler, H. "Position control in lithographic equipment". In: *IEEE Control Systems Magazine* 31.5 (2011), pp. 28–47.

[2] Bhikkaji, B. et al. "High-performance control of piezoelectric tube scanners". In: *IEEE Transactions on Control Systems Technology* 15.5 (2007), pp. 853–866.

[3] Bronowicki, A. J. "Vibration isolator for large space telescopes". In: *Journal of spacecraft and rockets* 43.1 (2006), pp. 45–53.

[4] Li, L. et al. "Micro-vibration suppression methods and key technologies for high-precision space optical instruments". In: *Acta Astronautica* 180 (2021), pp. 417–428.

[5] Schmidt, R.-H. M. "Ultra-precision engineering in lithographic exposure equipment for the semiconductor industry". In: *Philosophical Transactions of the Royal Society A: Mathematical, Physical and Engineering Sciences* 370.1973 (2012), pp. 3950–3972.

[6] Gordon, C. G. "Generic vibration criteria for vibration-sensitive equipment". In: *Optomechanical Engineering and Vibration Control*. Vol. 3786. SPIE. 1999, pp. 22–33.

[7] Poel, G. W. V. D. "An exploration of active hard mount vibration isolation for precision equipment". PhD thesis. University of Twente, May 2010.

[8] Amick, H. et al. "Evolving criteria for research facilities: vibration". In: *Buildings for Nanoscale Research and Beyond*. Vol. 5933. SPIE. 2005, pp. 16–28.

[9] Schmidt, R. M., Schitter, G., and Rankers, A. *The design of high performance mechatronics-: high-Tech functionality by multidisciplinary system integration*. Ios Press, 2020.

[10] Poel, T. V. D. et al. "Improving the vibration isolation performance of hard mounts for precision equipment". In: *IEEE/ASME International Conference on Advanced Intelligent Mechatronics, AIM* (2007).

[11] Beard, A. M., Schubert, D. W., and Flotow, A. H. von. "Practical product implementation of an active/passive vibration isolation system". In: *Vibration Monitoring and Control*. Vol. 2264. SPIE. 1994, pp. 38–49.

[12] Karnopp, D. "Active and Semi-Active Vibration Isolation". In: *Journal of Vibration and Acoustics* 117.B (June 1995), pp. 177–185.

[13] Zuo, L., Slotine, J.-J., and Nayfeh, S. A. "Experimental study of a novel adaptive controller for active vibration isolation". In: *Proceedings of the 2004 American Control Conference*. Vol. 4. IEEE. 2004, pp. 3863–3868.

[14] Balas, M. J. "Direct velocity feedback control of large space structures". In: *Journal of guidance and control* 2.3 (1979), pp. 252–253.

[15] Tjepkema, D., Dijk, J. V., and Soemers, H. M. "Sensor fusion for active vibration isolation in precision equipment". In: *Journal of Sound and Vibration* 331 (4 Feb. 2012), pp. 735–749.

[16] Preumont, A. et al. "Force feedback versus acceleration feedback in active vibration isolation". In: *Journal of sound and vibration* 257.4 (2002), pp. 605–613.

[17] Collette, C. and Matichard, F. "Sensor fusion methods for high performance active vibration isolation systems". In: *Journal of sound and vibration* 342 (2015), pp. 1–21.

[18] Goht, C. J. and Caugheys, T. K. "On the stability problem caused by finite actuator dynamics in the collocated control of large space structures". In: *Taylor and Francis* 41 (3 1985), pp. 787–802.

[19] Beijen, M. A. et al. "Self-tuning MIMO disturbance feedforward control for active hard-mounted vibration isolators". In: *Control Engineering Practice* 72 (Mar. 2018), pp. 90–103.

[20] Jabben, L and Van Eijk, J. "Performance analysis and design of mechatronic systems". In: *Mikroniek* 51.2 (2011), pp. 5–12.

[21] Collette, C., Janssens, S., and Artoos, K. "Review of active vibration isolation strategies". In: *Recent patents on Mechanical engineering* 4.3 (2011), pp. 212–219.

[22] GmbH, P. C. *Properties of Piezo Actuators — piceramic.com*. `https://www.piceramic.com/en/expertise/piezo-technology/properties-piezo-actuators`. [Accessed 30-03-2024].

[23] Beijen, M. A. et al. "Self-tuning Feedforward Control for Active Vibration Isolation of Precision Machines". In: *IFAC Proceedings Volumes* 47 (3 Jan. 2014), pp. 5611–5616.

[24] Hakvoort, W. B., Boerrigter, G. J., and Beijen, M. A. "Active vibration isolation by model reference adaptive control". In: vol. 53. Elsevier B.V., 2020, pp. 9144–9149.

[25] Beijen, M. et al. "H∞ feedback and feedforward controller design for active vibration isolators". In: *IFAC-papersonline* 50.1 (2017), pp. 13384–13389.

[26] Tjepkema, D. "Active hard mount vibration isolation for precision equipment". PhD thesis. 2012.

[27] Ridder, L. van de et al. "Coriolis mass-flow meter with integrated multi-DOF active vibration isolation". In: *Mechatronics* 36 (June 2016), pp. 167–179.

[28] Beadle, B. M. et al. "Active control strategies for vibration isolation". In: *IUTAM Symposium on Vibration Control of Nonlinear Mechanisms and Structures*. Springer. 2005, pp. 91–100.

A

Experimental Setup

Below more details regarding the setup will be given. First the components of the experimental setup will be named. Next the CompactRio and the Labview program used for data gathering and control signal calculations is described as well as some remarks on delay and system identification.

A.1. Detailed System Description

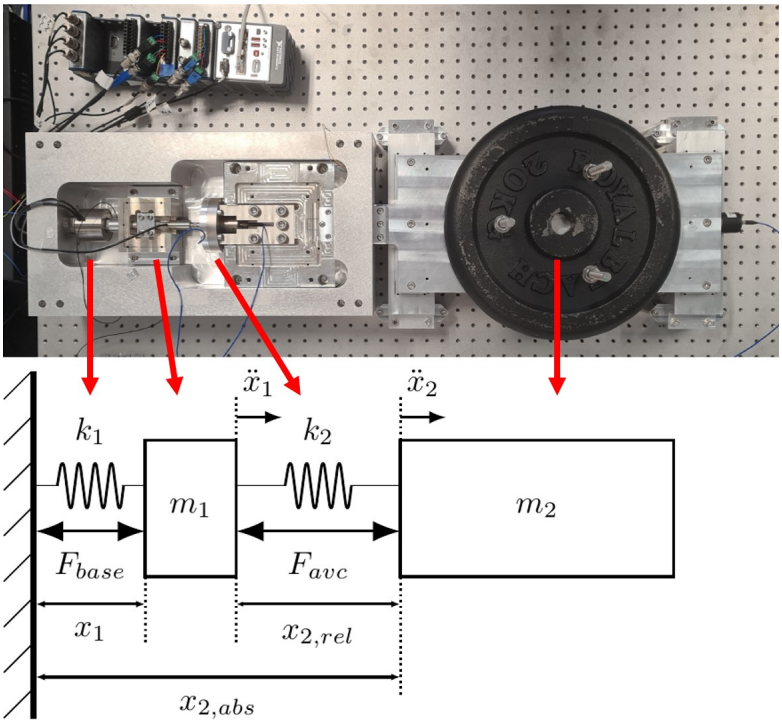

Figure A.1: Top-down view of the experimental setup with corresponding mass-spring model.

A single-axis experimental setup, shown in figure A.1, is used to represent an ultra hard mount system. A platform with adjustable mass represents the payload to be supported, indicated by m_2. This mass was chosen at 56kg such that the resonance frequency was 103Hz. By choosing a lower mass the frequency may be shifted to a higher frequency. The main stack actuator (model *P-843.20*), indicated by F_{avc} has a stiffness of 27×10^6 N/m, and constitutes the ultra hard mount and connects the payload to the shaking base, m_1. This shaking base is actuated by another stack actuator (model *P-235.15*), with a higher stiffness of 860×10^6 N/m, indicated by F_{base}. Motion of all elements of the setup is constrained to a single degree of freedom using flexures.

Accelerations $\ddot{x}_1, \ddot{x}_2$ are measured using *PCB Synotech 393B05* accelerometers. Absolute displacement of m_1 is measured with a *PIseca D-510.021* and the the absolute displacement of m_2 with a *D-050* capacitive sensor. Finally, relative measurements are taken with the integrated strain gauge sensors of the stack actuators.

The acceleration signal were passed through a *Synotech PCB-483C15* signal conditioning unit. Next all the measurement signals were filtered in an *E-712 Digital Piezo Controller*. The filtered signals were send to a CompactRio running Labview. Using the FPGA module of this CompactRio, control signals were calculated and send back to the E-712. After amplifying the control signal these were then send to the stack actuators to close the loop.

A.2. CompactRIO and Labview

The system was controlled using a CompactRIO running Labview 2023 Q3 (32-bit). The CompactRIO consists of a microprocessor, FPGA module and a frame that held the following sub-modules:

1. NI 9263 4-Channel Analog Output +- 10V, 16 bit resolution
2. NI 9215 4-Channel Analog Input +- 10V, 16 bit resolution
3. NI 9201 8-Channel Analog Input +- 10V, 12 bit resolution

Labview was used to take measurements, calculate control signals and send signals (identification, control and disturbance signals). In this section these three functionalities are elaborated upon.

The labview program is split in three 'Virtual Instruments'(VI) that have their own distinct function and are run on slightly different places. First the Host.vi runs locally on the connected computer. The host is used to plot data, send and receive files to and from the CompactRIO, and save (measurement) data locally. Secondly, RTmain.vi runs on the CompactRIO microprocessor and is used as a control panel to operate all the different functionalities such as: turning power on/off to the actuators, setting controller transfer functions, turning on/off control, sending disturbance signals to the system, and sending chirp signals to the system. Lastly, the FPGA.vi runs on the FPGA board of the CompactRIO and is used to gather inputs and send outputs from the sub-modules. It also calculates the control signals. The FPGA runs at a sampling frequency of 10.000 Hz.

A.2.1. Measurements with Labview

The following sensor signals are sent (filtered) from the E-712 to the CompactRIO:

- x_1 Absolute position of m_1
- $\ddot{x}_1$ Acceleration of m_1
- $x_{2,abs}$ Absolute position of m_2
- $\ddot{x}_2$ Acceleration of m_2
- ${x_1}^*$ Relative position of m_1
- $x_{2,rel}$ Relative position of m_2

These are then read by the FPGA module with the the NI-9215 and NI-9201 sub-modules. In Labview functionality is added to be able to zero-mean the signals to avoid unwanted offsets. In the FPGA.vi measurement data is gathered in an array and send to the Host.vi. In the host these signals are plotted and can be saved locally to a tab separated .lvm file. This .lvm can be read with Matlab to do data analysis. For example, the data was used to calculate transfer functions and used to calculate the performance with Dynamic Error Budgeting.

A.2.2. System Delay

As with any measurement and control signal the system has some sources of delay. It was found by matching the measured transfer function from control signal outputted from the CompactRio through the system back to the CompactRio input there is a delay of about 500 microseconds.

There are multiple sources adding to this delay. First there are two servo loops in the E-712 that add delay depending on the refresh rate. In this case it can be assumed that these add about 100 microseconds of

delay to the system. The signal conditioning unit may have another 50 microseconds. Therefore, using Labview for external control adds about 250 microseconds, in this case doubling the total amount of delay. For feedback this was not found to have an impact on performance. However, this delay did limit the effectiveness of feedforward.

A.2.3. System Identification

Good knowledge of the system is essential for effective control. As such, intensive system identification was performed on the setup using Labview. By measuring the output of a system from a known input or by comparing two inputs, the transfer function between two signals can be calculated. It is important that the signal-to-noise (s-to-n) ratio is high enough to find the correct relation. Theoretically any signal that includes the frequencies that are to be identified will work. Noise signals, or step inputs are easy to implement signals that can be used. However, better results were obtained by using a chirp signal. A chirp signal is a sinusoidal wave with increasing frequency as time passes. This is a very effective signal for identification because each frequency is excited individually one-by-one. The amplitude can be increased to have good s-to-n ratio. However, the input must not be too high to avoid exciting the modes of the system too much and damaging the system. This makes a chirp signal potentially risky for all modes are excited individually and for a prolonged time.

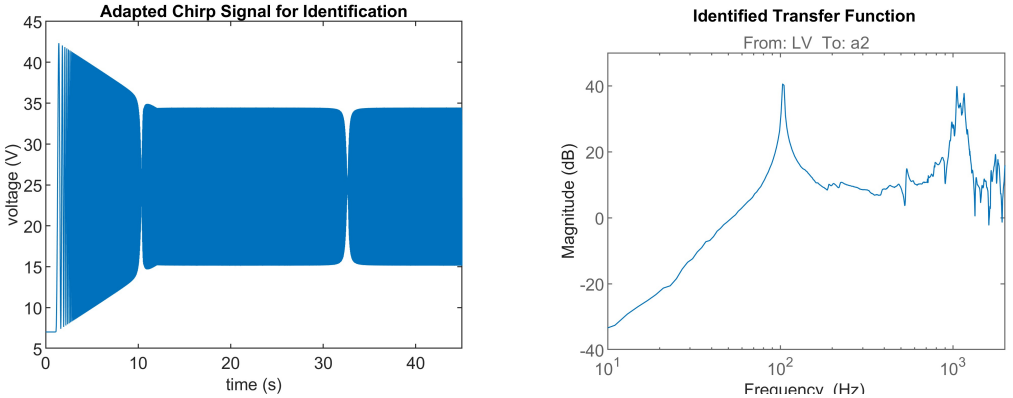

(a) Adapted chirp, the first resonance around 100 Hz and the peak at around 1000 Hz has been notched away

(b) Example of identified transfer function from avc actuator control signal to acceleration of second mass

Figure A.2: An example of identified transfer function and corresponding adapted chirp signal. At around 10 seconds the chirp has a frequency of 100 Hz, corresponding to the first mode of the system. To avoid damaging the system, the amplitude has been decreased with a notch filter. Likewise, the amplitude at frequencies 1000 - 1100 has been decreased as well.

To improve identification results and avoid damage certain adaptions can be made to a chirp signal. First, after making a noisy identification using a safe chirp signal with low amplitude, the frequencies of the biggest modes can be determined. Subsequently, the amplitude of the excitation signal can be decreased at these frequencies with notch filters, while the amplitude for every other frequency is slightly increased. If the identification is repeated with this new signal, it should be less noisy. By repeating this process until the s-to-n ratio is high at all frequencies, a good identification should be possible. Nevertheless, plant dynamics may still prevent a good s-to-n ratio for every frequency. For example, the transfer function from actuator voltage to position gives a low-pass behaviour, with a -2 slope after the resonance. In order, to get a good s-to-n ratio in the frequency regions were the signals are damped by the system an increase in excitation signal amplitude is needed, but for the other frequencies this is undesired to avoid exciting eigenmodes. Thus, a second improvement is to increase chirp signal amplitude were the plant response decreases. In Figure A.2 an example of system and corresponding tuned chirp signal.

A.2.4. Control Signal Calculation

Control signal calculation is done using the FPGA module on the CompactRio. FPGA is short for 'field-programmable gate array'. A FPGA is a configurable integrated circuit consisting of arrays of logic blocks that can be reprogrammed after manufacturing. As the gates are programmed physically after compilation of the code this ensures very fast calculations. This enables control calculations at 10 kHz in

the case of this CompactRio. Functionality was added such that the control signal could be chosen from any of the measurement signals. The control signals of the feedback and feedforward signals are added before outputting through the NI-9263 module. This signals is send through the E-712 for amplification to the stack actuators.

B

Gain Sweeps of Feedback Controllers

Gain sweeps were performed for each controller to find suitable gains. Below the results for each feedback controller can be found in figure B.1. For each controller five results are plotted around the chosen gain to illustrate the effect of gain on the total error for each approach. The influence of gain is discussed in depth in Chapter 3. For each of the feedback methods there is a clear trade-off between damping and noise amplification. At some point increasing the gain further leads to such an increase in noise amplification that the extra damping does not compensate. By increasing the gain slowly until such point was reached, the best controller gain was found experimentally.

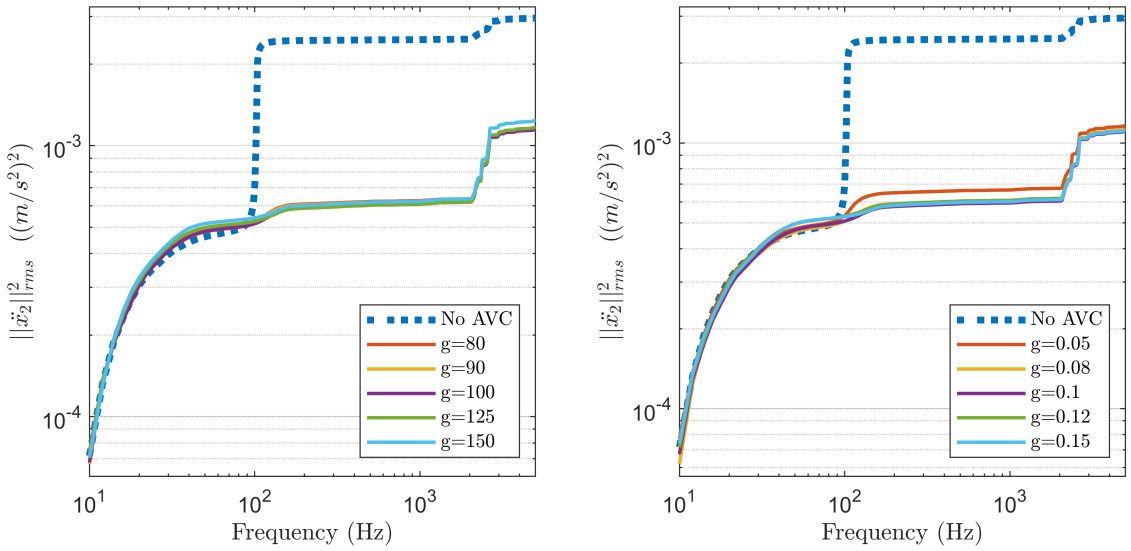

(a) Gain Sweep Velocity Feedback

(b) Gain Sweep Velocity Bandpass Feedback

Figure B.1: Gain Sweeps for each of the feedback controllers. For each approach 5 results are shown.

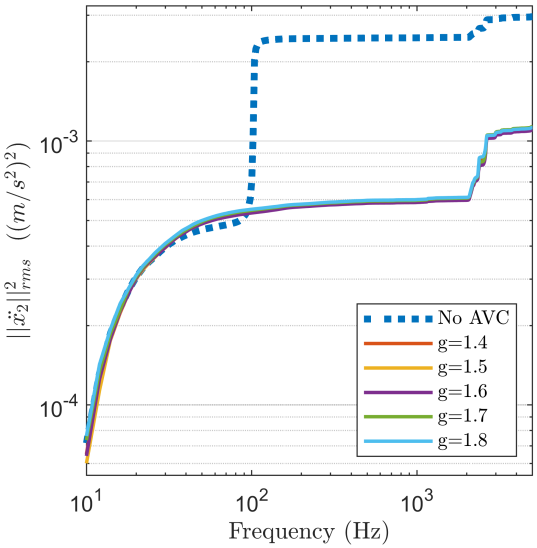

(c) Gain Sweep Negative Acceleration Feedback

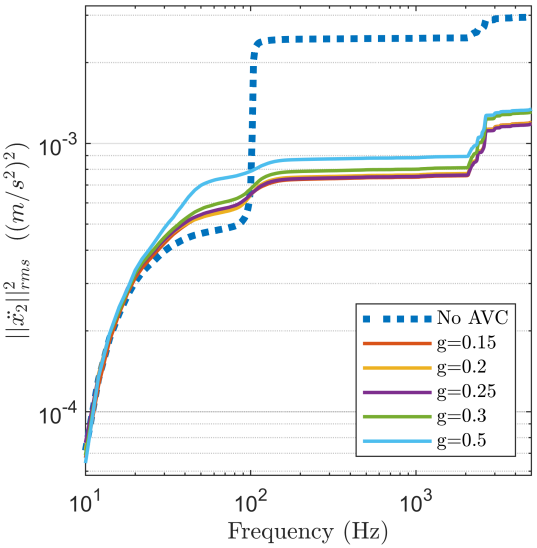

(d) Gain Sweep Absolute Positive Position Feedback

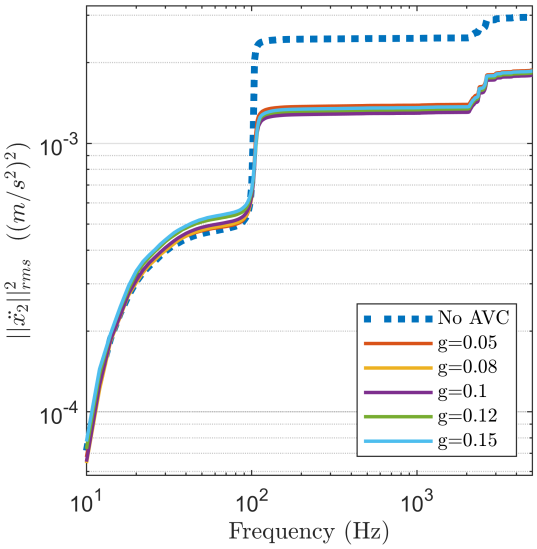

(e) Gain Sweep Relative Positive Position Feedback

Figure B.1: Gain Sweeps for each of the feedback controllers. For each approach 5 results are shown.

C

Floor Dominated Disturbance Case

In the thesis the disturbances were based on the VC-C curve and a force profile provided by PI, shown in Chapter 1. It was briefly investigated how the dynamics of the disturbance sources influence the relative performance of the controllers. To find out the comparison was also done with a disturbance case in which the floor vibrations were dominant.

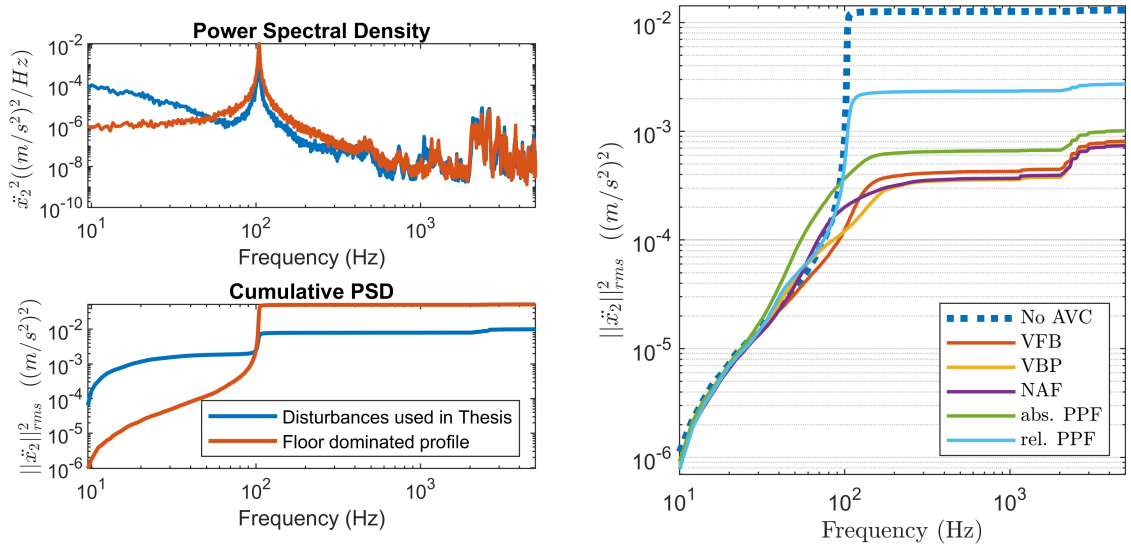

(a) PSD and CPS of the output with the disturbances used in this thesis and with a different floor vibration dominated disturbance spectrum. **(b)** Results of feedback controllers, with gains tuned to this spectrum.

Figure C.1: Results with a floor dominated disturbance case

S

In figure C.1a the power spectra of the output with the disturbance profile that was used in the thesis and a different one can be found. With this different spectrum the force disturbance is smaller, and the floor disturbance is bigger. This is not an application where an ultra hard mount would excel, but where a softer mount would probably be used. However, in C.1b, it can be seen that damping performance is still excellent. Comparing to the results of the standard disturbance profile, the relative performance does not change. The acceleration-based controllers outperform the displacement-based controllers as they can reach higher levels of damping without amplifying as much low frequency noise. At the cost of more elaborate tuning the Velocity Bandpass Feedback and Negative Acceleration Feedback controllers have a bit higher performance than Velocity Feedback.

D

Dynamic Error Budgeting

In this section the Dynamic Error Budgeting (DEB) method for calculating the influence of disturbances on an output is explained. First the general theory behind DEB will be given. Next a method of using DEB simulation for optimization purposes will be provided.

D.1. Theory behind DEB

Dynamic Error Budgeting was used mainly as a performance metric in this Thesis. DEB is used to derive the total error from its different contributing components. As an analysis tool it is very effective to show which frequencies contribute most to the total error. This makes it a powerful tool in the design phase of systems or controllers, as it avoids wasted efforts to factors contributing less to total error. In this section the method of Dynamic Error Budgeting, as introduced in [20] and described in more detail in [9, Chapter 8.1], will be explained.

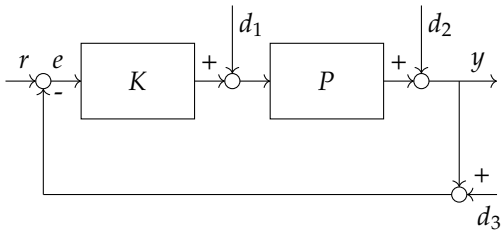

Figure D.1: Closed-loop schematic with different disturbances with plant P, controller K, noise sources d_1, d_2, d_3, and output y

The relation from disturbance source to output is given by their respective power spectra and the transfer function from input to output. The total error is given by the sum of the disturbance sources as follows:

$$\mathrm{PSD}_y(f) = \sum_i \mathrm{H}_i(f)^2 \cdot \mathrm{PSD}_{d_i}(f) \ ,$$

where PSD_y and PSD_{d_i} are the power spectra of the output and disturbance sources respectively, and $H_i(f)$ is the transfer function between each input and the output.

For the DEB approach to be valid, the following assumption must be true:

- All subsystems can be accurately described by a linear time-invariant model.
- The statistical properties of the disturbances do not change over time.
- The disturbances are all stochastic.

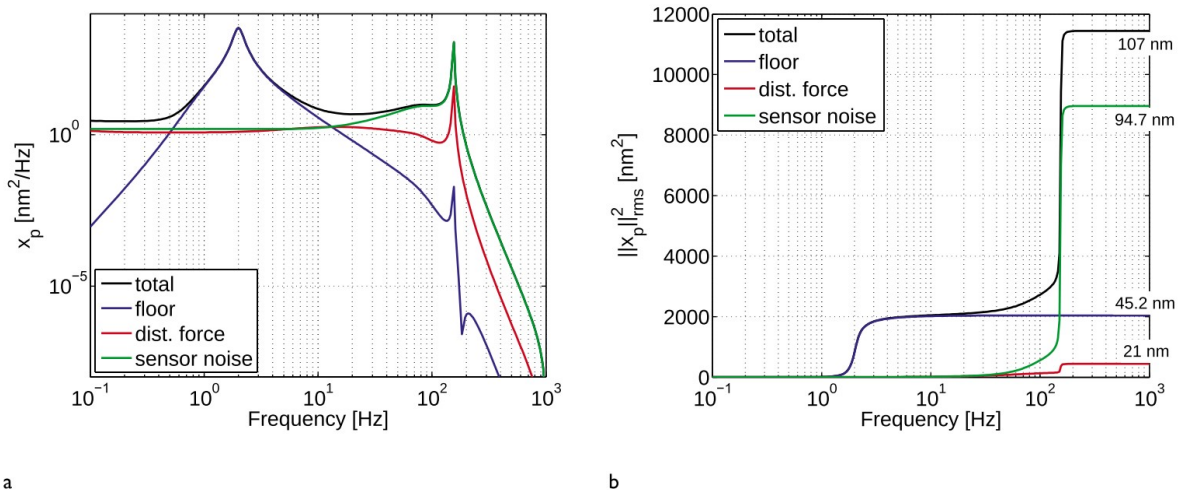

Figure D.2: An example of Dynamic Error Budgeting from [20] showing the PSD (fig. a) and CPS (fig. b). The dynamics of the output signal from each disturbance input can be seen clearly in the PSD. However, it is hard to judge the influence of different peaks on the total error, or see what that total error is. For this reason, the CPS plot may be used which clearly shows the contribution to the error at each frequency and the total error.

It can be difficult to judge the influence on the total error of different peaks at different frequencies. Therefore it is convenient to use the Cumulative Power Spectrum (CPS). The CPS is calculated using the following formula:

$$\mathrm{CPS}(f) = \int_0^f \mathrm{PSD}(v)\,\mathrm{d}v$$

The CPS increases with frequency and the final value of the CPS is equal to the square of the RMS of the output signal. It shows visually the contribution of each frequency to the total error. In the context of AVC, the effect of resonance modes can be observed for example, and the effect of damping. It is discouraged to directly take the square of the CPS and plot a 'Cumulative Amplitude Spectrum'. Doing this unfairly visually enlarges the lower frequency contribution of disturbances relative to the higher frequency contributions. This may focus attention to the wrong disturbance resulting in wrong decisions.

D.2. Simulated DEB for Optimization

Instead of measuring the output signal and directly calculating the PSD and CPS to find the error. DEB can also be used for predicting the performance. For this accurate models of the transfer functions between each disturbance and the output are required. Furthermore, intimate knowledge of each of the disturbance sources and their dynamics are needed.

It was briefly tried to create dynamic error budgeting model of the plant to use it for optimization of the controllers. However, it was found that the models couldn't accurately capture the dynamics of the high-frequency modes. It was found experimentally that these modes impact the performance drastically. Increasing the controller gain led to a reduced stability margin, increasing the noise at these frequencies. The linearized model couldn't accurately predict this behaviour. As such it was not a useful tool for optimization for this thesis, and instead a manual gain sweep was used to find suitable controller gains.

If it had been possible to capture the dynamics of the system well, and the calculated closed loop response did match reality well, optimization would have been done as follows. An optimization algorithm could have been employed such as a rough grid search or a more elegant algorithm. Such an algorithm can change the parameters of a controller and use the DEB model to calculate the CPS and thereby find the total error. Not only the controller gain can be optimized in such fashion but also other

parameters, like the corner frequencies of the Velocity Bandpass feedback controller. In this fashion an optimally tuned controller can be found for very specific disturbance cases. If the goal of a project is to achieve the best possible performance, or be able to quickly find optimal controllers for different disturbance cases it may be worthwhile to investigate this further.